



RESEARCH ARTICLE

10.1029/2021JD034859

The Role of Natural Halogens in Global Tropospheric Ozone Chemistry and Budget Under Different 21st Century Climate Scenarios

Key Points:

- Water vapor and iodine are key drivers of future tropospheric ozone destruction
- Natural halogens reduce 30–35 Tg of tropospheric ozone burden throughout the 21st century regardless of the Representative Concentration Pathway scenario considered
- Enhanced halogen-driven surface ozone loss will determine the effectiveness of future policies on air quality

Supporting Information:

Supporting Information may be found in the online version of this article.

Correspondence to:

A. Saiz-Lopez,
a.saiz@csic.es

Citation:

Badia, A., Iglesias-Suarez, F., Fernandez, R. P., Cuevas, C. A., Kinnison, D. E., Lamarque, J.-F., et al. (2021). The role of natural halogens in global tropospheric ozone chemistry and budget under different 21st century climate scenarios. *Journal of Geophysical Research: Atmospheres*, 126, e2021JD034859. <https://doi.org/10.1029/2021JD034859>

Received 4 MAR 2021

Accepted 27 SEP 2021

Alba Badia^{1,2} , Fernando Iglesias-Suarez^{1,3} , Rafael P. Fernandez^{1,4} , Carlos A. Cuevas¹ , Douglas E. Kinnison⁵ , Jean-Francois Lamarque⁶ , Paul T. Griffiths^{7,8} , David W. Tarasick⁹ , Jane Liu¹⁰ , and Alfonso Saiz-Lopez¹

¹Department of Atmospheric Chemistry and Climate, Institute of Physical Chemistry Rocasolano, CSIC, Madrid, Spain, ²Now at Institute of Environmental Science and Technology (ICTA), Universitat Autònoma de Barcelona (UAB), Barcelona, Spain, ³Deutsches Zentrum für Luft- und Raumfahrt (DLR), Institut für Physik der Atmosphäre, Weßling, Germany, ⁴Institute for Interdisciplinary Science (ICB), National Research Council (CONICET), FCEN-UNCuyo, Mendoza, Argentina, ⁵Atmospheric Chemistry, Observations, and Modeling Laboratory, NCAR, Boulder, CO, USA, ⁶Climate and Global Dynamics Laboratory, NCAR, Boulder, CO, USA, ⁷Centre for Atmospheric Science, Cambridge University, Cambridge, UK, ⁸National Centre for Atmospheric Science, Cambridge University, Cambridge, UK, ⁹Air Quality Research Division, Environment and Climate Change Canada, Downsview, ON, Canada, ¹⁰Department of Geography and Planning, University of Toronto, Toronto, ON, Canada

Abstract Tropospheric ozone (O₃) is an important greenhouse gas and a surface pollutant. The future evolution of O₃ abundances and chemical processing are uncertain due to a changing climate, socioeconomic developments, and missing chemistry in global models. Here, we use an Earth System Model with natural halogen chemistry to investigate the changes in the O₃ budget over the 21st century following Representative Concentration Pathway (RCP)6.0 and RCP8.5 climate scenarios. Our results indicate that the global tropospheric O₃ net chemical change (NCC, chemical gross production minus destruction) will decrease ~50%, notwithstanding increasing or decreasing trends in ozone production and loss. However, a wide range of surface NCC variations (from -60% to 150%) are projected over polluted regions with stringent abatements in O₃ precursor emissions. Water vapor and iodine are found to be key drivers of future tropospheric O₃ destruction, while the largest changes in O₃ production are determined by the future evolution of peroxy radicals. We show that natural halogens, currently not considered in climate models, significantly impact on the present-day and future global O₃ burden reducing ~30–35 Tg (11–15%) of tropospheric ozone throughout the 21st century regardless of the RCP scenario considered. This highlights the importance of including natural halogen chemistry in climate model projections of future tropospheric ozone.

1. Introduction

Tropospheric ozone (O₃) is of particular interest for global climate and air quality due to its key role as a radiatively active gas, an oxidizing agent and a surface pollutant in urban areas, where it is a major component of the photochemical smog that causes a variety of health effects (Anenberg et al., 2010; Murray et al., 2020; Sillman, 2003). Indeed, it has been estimated that 365,000 respiratory mortalities worldwide in year 2019 were due to anthropogenic O₃, representing ~16% increase with respect to year 2010 (314,000) (Murray et al., 2020). As a greenhouse gas, O₃ is currently considered the third most important anthropogenic greenhouse gas, contributing a global radiative forcing of $\sim 0.40 \pm 0.2 \text{ Wm}^{-2}$ with a 5–95% confidence interval (Myhre et al., 2013).

Tropospheric O₃ is primarily produced as a secondary photochemical oxidation product of methane (CH₄), carbon monoxide (CO), and non-methane volatile organic compounds (NMVOCs) in the presence of nitrogen oxides (NO_x = NO + NO₂) (Crutzen, 1974; Derwent et al., 1996; Monks et al., 2015). Another important source of tropospheric O₃ is the downward transport from the stratosphere (stratosphere-troposphere transport, STT) (Hsu & Prather, 2009; Stohl et al., 2003), following O₃ production from photolysis of oxygen (O₂) molecules. In addition to surface deposition, tropospheric O₃ loss processes include photochemical reactions involving water vapor (H₂O), hydroxyl radical (OH), hydroperoxyl (HO₂), and reactive halogens

© 2021. The Authors.

This is an open access article under the terms of the [Creative Commons Attribution-NonCommercial-NoDerivs License](https://creativecommons.org/licenses/by/4.0/), which permits use and distribution in any medium, provided the original work is properly cited, the use is non-commercial and no modifications or adaptations are made.

(chlorine, bromine, and iodine). Besides emissions of O₃ precursors and depleting substances, climate change will also be a key driver of future global tropospheric O₃ abundance and distribution (Iglesias-Suarez et al., 2018; Young et al., 2018).

Global warming will increase future atmospheric stagnation events that build up surface O₃ levels, worsening air quality (Archer et al., 2019). On the other side, enhanced tropospheric water vapor concentrations—due to global warming—will lead to increasing reaction with excited oxygen atoms, one of the main routes for tropospheric O₃ loss and OH production (Brasseur et al., 1998; Johnson et al., 1999; Stevenson et al., 2000). Future changes in land cover, temperature, turbulence, relative humidity, and soil moisture will impact on surface O₃ deposition rates (Ganzeveld et al., 2010), with implications for both air quality and ecosystem productivity. Moreover, numerous studies have highlighted the key role that STT—enhanced under climate change due to a stronger Brewer-Dobson circulation—plays in the global tropospheric O₃ burden, with significant increases in the subtropical and extratropical upper free troposphere (Banerjee et al., 2016; Butchart, 2014; Collins et al., 2003; Neu et al., 2014; Sudo et al., 2003).

Previous modeling studies have attempted to provide estimates of the future evolution of tropospheric O₃ under different emissions scenarios and climate change based on time-slice simulations (Banerjee et al., 2016; Iglesias-Suarez et al., 2018; Young et al., 2013; Zeng et al., 2008). A complete review can be found in the framework of the Tropospheric Ozone Assessment Report (TOAR) activity (Archibald, Neu, et al., 2020; Gaudel et al., 2018; Schultz et al., 2017; Tarasick et al., 2019; Young et al., 2018) an international scientific assessment of the global distribution and trends of tropospheric ozone. Data sets derived from five satellite measurements provide a global tropospheric ozone burden about of ~300 Tg between 60°N and 60°S for years 2014–2016 (Gaudel et al., 2018). In addition, observational data sets from ozonesondes (Trajectory-mapped Ozonesonde data set for the Stratosphere and Troposphere, TOST [G. Liu, Liu, et al., 2013; J. Liu, Tarasick, et al., 2013]) have been recently compared with data from Phase 6 of the Coupled Model Intercomparison Project (CMIP6) models (Griffiths et al., 2021).

Here, we use a state-of-the-art Earth System Model (Tilmes et al., 2016) with natural halogen chemistry to investigate the response of the tropospheric O₃ budget and chemistry to changes in climate and precursors emissions, both natural and anthropogenic, between 2000 and 2099. This is the first detailed timeline analysis of the future evolution of the main individual chemical production and loss terms that determine the O₃ budget under a changing climate, including both the surface and within the troposphere global trends during the 21st century, as well as the regional spatio-temporal variability for the main O₃ depleting and production families. Two projected emissions scenarios of the Representative Concentration Pathway (RCP, namely RCP6.0 and RCP8.5) (Meinshausen et al., 2011; van Vuuren et al., 2011) are used.

2. Methods

2.1. CESM (CAM-Chem) Model

The Community Earth System Model (CESM; version 1.1.1), with the Community Atmospheric Model including interactive chemistry (CAM-Chem; version 4), was used to explore the tropospheric ozone chemistry and its budget over the 21st century (see Table S1 in Supporting Information S1 for a list of reactions included in the model). The model extends from the surface to ~40 km (3.5 hPa in the upper stratosphere) with 26 levels (18 levels below 100 hPa) and includes a horizontal resolution of 1. × 2.5° (latitude × longitude). The benchmark chemical scheme in CAM-Chem represents 169 species with comprehensive photochemistry (gas-phase and heterogeneous reactions) coupled to the radiation scheme (Tilmes et al., 2016). In addition, the chemical mechanism here includes a state-of-the-art halogen photochemistry scheme, considering wet and dry deposition for naturally emitted halogens (containing chlorine, bromine, and iodine) as well as heterogeneous recycling in the troposphere and stratosphere. The implemented geographically variant and temporally dependent natural halogen sources include both, biogenic and abiotic routes, and are described elsewhere (Fernandez et al., 2014; Ordóñez et al., 2012; Saiz-Lopez et al., 2014, 2015). Briefly, biogenic sources comprise nine halocarbons (CHBr₃, CH₂Br₂, CH₂BrCl, CHBr₂Cl, CHBrCl₂, CH₃I, CH₂I₂, CH₂I₂Br, and CH₂I₂Cl), which are the result of phytoplankton and (micro-) macroalgae metabolism and photochemistry at the ocean's surface (Ordóñez et al., 2012). Abiotic iodine source gas (HOI and I₂) emissions are directly emitted from the ocean as a consequence of O₃ deposition and reactions with seawater iodide

(Prados-Roman et al., 2015). This abiotic route is dependent on surface O₃ concentration, wind speed and sea surface temperature (SST) (Carpenter et al., 2013; MacDonald et al., 2014). Note that, inorganic iodine emissions in this work might be considered as a lower limit due to the parameterization used here (MacDonald et al., 2014) results in lower *aq*] compared with other studies (Chance et al., 2014) and electronic affinity between O₃ and iodide is not considered.

The model climatological set-up is identical to the Chemistry-Climate Model Initiative REFC2 experiment (transient simulation between 1960 and 2100) (Morgenstern et al., 2017). Future (2006–2100) projections followed the emission scenarios RCP6.0 and RCP8.5 (Meinshausen et al., 2011; van Vuuren et al., 2011). Monthly and seasonally varying boundary conditions were specified for CO₂, N₂O, CH₄, as well as for long-lived halogen-containing species (CH₃Cl, CH₃CCl₃, CCl₄, CFC-11, CFC-12, CFC-113, HCFC-22, CFC-114, CFC-115, HCFC-141b, HCFC-142b, CH₃Br, H-1301, H-1211, H-1202, and H-2402) following the A1 halogen scenario (WMO, 2011). Modeled present-day O₃—represented in CAM-Chem with an equivalent experimental set-up—has been evaluated against a number of observational data sets (Tilmes et al., 2016).

2.2. Model Validation

Data from TOST (G. Liu, Liu, et al., 2013; J. Liu, Tarasick, et al., 2013) and TOAR (Archibald, Neu, et al., 2020; Gaudel et al., 2018; Schultz et al., 2017; Tarasick et al., 2019; Young et al., 2018) activities are used for the modeled ozone burden validation.

TOST has been evaluated using independent ozone soundings (not included in the climatology) by backward and forward trajectory comparisons, and by comparisons with aircraft profiles and surface monitoring data (G. Liu, Liu, et al., 2013; J. Liu, Tarasick, et al., 2013; Tarasick et al., 2010). Differences are typically about 10% or less, but there are larger biases in the UTLS, the boundary layer, and in areas where ozone-sonde measurements are very sparse. The accuracy of the TOST product depends largely on the accuracy of HYSPLIT and the meteorological data used. The calculations of tropospheric ozone burden (total column ozone integrated over the globe) presented here use the full-profile TOST data set that includes trajectories originating in the stratosphere.

The TOST data set was compiled from global observations while the TOAR data set includes measurements from satellite-borne instruments (Gaudel et al., 2018): Ozone Monitoring Instrument (OMI)/Microwave Limb Sounder, Global Ozone Monitoring Experiment (GOME) and OMI-Smithsonian Astrophysical Observatory, OMI-Rutherford Appleton Laboratory, Infrared Atmospheric Sounding Interferometer (IASI)-Fast Optimal Retrievals on Layers, IASI-Software for a Fast Retrieval of IASI Data, IASI-Laboratoire Interuniversitaire des Systèmes Atmosphériques, IASI + GOME-2, and Scanning Imaging Absorption Spectrometer for Atmospheric Chartography.

2.3. Model Comparison

The CMIP6 model data presented here are taken from the recent overview by Griffiths et al. (2021) which uses data from the CMIP Historical and ScenarioMIP ssp370 experiments from UKESM1 (Sellar et al., 2019), GFDL-ESM4 (Krasting et al., 2018), CESM2-WACCM (Danabasoglu, 2019), and MRI-ESM-2 (Yukimoto et al., 2019). The tropospheric ozone burden was calculated using archived monthly mean data from the AERmon archive of tropospheric O₃ mixing ratio on native model grids, along with data on the tropopause pressure using the WMO definition of the tropopause (CMIP6 ptp variable).

2.4. Model Runs

A total of four different simulations were performed in this study that uses the two projected emissions scenarios RCP6.0 and RCP8.5 (Meinshausen et al., 2011; van Vuuren et al., 2011). The first set of simulations (HAL RCP6.0 and HAL RCP8.5) uses the RCP6.0 and RCP8.5 emission scenarios, respectively, and include a state-of-the-art halogen chemistry (anthropogenic and natural). Since the natural halogens emissions are dependent on climate-related factors, halocarbon and inorganic iodine fluxes will vary as climate changes. Our simulations are identical to the ones described by Iglesias-Suarez et al. (2020) using the projected very short-lived halocarbons natural source based on the evolution of physical (SST, salinity) and

biogeochemical (marine net primary production) drivers related to climate. Note that the contribution from anthropogenic very short-lived chlorine species (Hossaini et al., 2016, 2019) has not been considered here. Abiotic iodine source gas (HOI and I₂) emissions are also dependent on climate factors (wind speed and SSTs). Present-day VSL halocarbons fluxes account for 1,121 Gg yr⁻¹ with an increase by ~7% and ~14% for the RCP6.0 and RCP8.5 scenarios, respectively, by the end of the century (Figure S1a in Supporting Information S1). Present-day inorganic iodine fluxes account for 2,667 Gg yr⁻¹, with an increase of ~20% following RCP8.5, and a decrease of ~10% for RCP6.0 (Figure S1b in Supporting Information S1). More information regarding the natural halogens emissions is provided in Iglesias-Suarez et al. (2020). The second set of simulations, referred here to NONATHAL RCP6.0 and NONATHAL RCP8.5, neglect tropospheric natural halogen chemistry (VSL chemistry, VSL halocarbons, and inorganic iodine source gas) and are only used for the computation of the global tropospheric ozone burden change with respect to the HAL simulations.

2.5. Odd Oxygen Definition

Several studies calculate the budget of odd oxygen (O_x) to account for species that rapidly interconvert with O₃. In this study, due to the nonlinearity of the O₃ photochemistry, we calculate the O_x budget instead of O₃ budget which is defined as:

$$O_x = O(^3P) + O(^2D) + O_3 + NO_2 + 2 \times NO_3 + HNO_3 + HO_2NO_2 + 3 \times N_2O_5 + PAN + MPAN + ONIT + ISO-PNO_3 + XO + HOX + XNO_2 + 2 \times XNO_3 + 2 \times OIO + 2 \times I_2O_2 + 3 \times I_2O_3 + 4 \times I_2O_4 + 2 \times OCIO,$$

where X = Cl, Br and I; PAN = peroxyacetyl nitrate, MPAN = methacryloyl peroxyxynitrate; ONIT = organic nitrate; ISOPNO₃ = peroxy radical from NO₃+isoprene.

Ozone accounts for the majority of O_x (99%). Therefore, hereafter we refer to the O₃ budget instead of O_x budget, which consists of four terms: gross chemical production (P), gross chemical loss (L), deposition to the surface (D), and STT.

Gross chemical production is defined as:

$$r(HO_2 + NO) + r(CH_3O_2 + NO) + r(PO_2 + NO) + r(CH_3CO_3 + NO) + r(C_2H_5O_2 + NO) + 0.92 \times r(ISOPO_2 + NO) + r(MACRO_2 + NOa) + r(MCO_3 + NO) + r(C_3H_7O_2 + NO) + r(XO_2 + NO) + 0.9 \times r(TOLO_2 + NO) + r(Other RO_2 + NO) + r(TERPO_2 + NO) + 0.9 \times r(ALKO_2 + NO) + r(ENEO_2 + NO) + r(EO_2 + NO) + r(MEKO_2 + NO) + 0.4 \times r(ONITR + OH) + r(J_{ONITR})$$

Gross chemical loss families are defined as:

$$Ox_{loss} = 2 \times r(O+O_3) + r(O^1D) + H_2O$$

$$NO_{loss} = 2 \times r(NO_2+O) + 2 \times r(J_{NO_3b})$$

$$HOx_{loss} = r(HO_2+O) + r(HO_2 + O_3) + r(OH + O) + r(OH + O_3) + r(H + O_3)$$

$$Halogen_{loss} (BrOx_{loss} + BrOx-ClOx_{loss} + ClOx_{loss} + IOx_{loss}) = 2 \times r(ClO + O) + 2 \times r(J_{Cl_2O_2}) + 2 \times r(ClO + ClOa) + 2 \times r(ClO + ClOb) + r(ClO + HO_2) + 2 \times r(BrO + BrO) + 2 \times r(BrO + O) + r(BrO + HO_2) + 2 \times r(BrO + ClOb) + 2 \times r(BrO + ClOc) + 2 \times r(IO + O) + 2 \times r(J_{OIO}) + r(IO*HO_2) + 2 \times r(IO + BrOa) + 2 \times r(IO + ClOb) + 2 \times r(IO + ClOc)$$

$$Other O_{loss} = r(C_3H_6 + O_3) + 0.9 \times r(ISOP + O_3) + r(C_2H_4 + O_3) + 0.8 \times r(MVK + O_3) + 0.8 \times r(MACR + O_3) + C_{10}H_{16} + O_3 + r(N_2O_5-aer) + r(NO_3-aer) + 0.5 \times r(NO_2-aer) + r(NO_3 + HO_2) + r(MACRO_2 + NO_3) + r(MCO_3 + NO_3) + r(ISOPO_2 + NO_3) + r(XO_2 + NO_3)$$

Dry deposition is computed considering all species that belong to the O_x family:

O₃ dry deposition = D(O₃) + 2 × D(I₂O₂) + 3 × D(I₂O₃) + 4 × D(I₂O₄) + (O_{3mw}/N_{mw}) × 1.25 × D(NO_y), where NO_y (=NO₂ + HNO₃ + HO₂NO₂ + PAN + MPAN + ONIT + ONITR + 2 × ClONO₂ + 2 × BrONO₂ + 2 × IONO₂) deposition term was normalized to both, O₃ molecular weight (O_{3mw}/N_{mw}) and 1.25 to account for the different species masses.

STT is calculated as the residual of the other terms (STT = D-[P-L]) (Stevenson et al., 2006). The tropospheric O₃ net chemical change (NCC) is the combination of the two chemical terms (NCC=P-L), which

Table 1

Changes in Tropospheric O₃ Burden and Budget During the 21st Century: Production (P), Loss (L), Net Chemical Change (NCC), Deposition (D), Stratosphere-Troposphere Transport (STT), Burden (B), and Tropospheric Chemical O₃ Lifetime ($\tau_{O_3} = B/[D + L]$)

	Present-day	Future (RCP6.0)	Future (RCP8.5)
HO ₂ +NO	3,006	2,570 (−15%)	3,079 (2%)
RO ₂ +NO	1,786	1,657 (−7%)	2,254 (26%)
Total chemical source (P)	4,792	4,227 (−12%)	5,334 (11%)
O _x _{loss}	1,991	1,923 (−3%)	2,417 (21%)
NO _x _{loss}	12	8 (−33%)	12 (0%)
HO _x _{loss}	1,468	1,320 (−10%)	1,701 (16%)
Halogens _{loss}	649	604 (−7%)	709 (9%)
Other O _x _{loss}	129	146 (13%)	191 (48%)
Total chemical loss (L)	4,250	4,001 (−6%)	5,030 (18%)
NCC (P−L)	542	226 (−58%)	304 (−44%)
O ₃ dry deposition (D)	873	694 (−21%)	820 (−6%)
O ₃ STT (D−[P−L])	331	468 (41%)	516 (56%)
O ₃ burden (Tg O ₃)	293	272 (−7%)	317 (8%)
O ₃ burden (Tg O ₃ , 125 ppbv contour of O ₃)	280	260 (−7%)	303 (8%)
O ₃ burden (Tg O ₃ , WMO tropopause [Reichler et al., 2003])	297	281 (−5%)	337 (13%)
O ₃ lifetime (days)	20.9	21.2	19.8

Note. All quantities consider the chemical tropopause defined by 150 ppbv contour of O₃. Ozone burdens using the chemical tropopause defined by 125 ppbv contour of O₃ and the WMO tropopause (Reichler et al., 2003) definition are also shown. Units are in Tg/yr unless stated differently. The percentage of increase/decrease by the end of the century (2090–2099) respect to the present-day (2000–2009) is shown in parentheses for each term. See Emmons et al. (2010), Lamarque et al. (2012), and Section 2 for further details on the definition of species and reaction rates (Sander et al., 2011). RCP, Representative Concentration Pathway.

is of major importance to the tropospheric O₃ budget and has been discussed previously in the literature (Fishman et al., 1979; Wild, 2007; Zeng et al., 2008).

3. Results and Discussion

Throughout this work, and unless stated otherwise, we present differences between the future-time or end of the century (defined as the 2090–2099 climatological mean) and the present-day (defined as the climatological mean for the 2000–2009) periods for two different scenarios: RCP6.0 and RCP8.5. Global integrated tropospheric values have been computed, in most cases, considering the model chemical tropopause (150 ppbv contour of O₃) (Stevenson et al., 2006; Young et al., 2013), while surface values refer to lower model levels with pressure >850 hPa. Uncertainties in the tropopause definition are reflected on the total tropospheric O₃ burden calculation (Archibald, Neu, et al., 2020; Gaudel et al., 2018; Griffiths et al., 2021). Therefore, the tropospheric O₃ burden calculation using different tropopause definitions is given at Table 1. A complete definition of the main chemical channels defining the gross chemical production (P), gross chemical loss (L) and the O₃ NCC (NCC = P−L) is provided in Table 1. The present-day global tropospheric levels for reactive inorganic chlorine, bromine, and iodine is 2.7, 1.8, and 1.0 pptv including natural sources and 9.6, 1.9, and 1.0 pptv including both anthropogenic and natural sources. Reactive halogen concentrations increase by 4–10% by 2100 with bromine driving this increase for RCP6.0 and both bromine and iodine for RCP8.5. Additional details regarding the halogen budget and trends for these model runs is provided in Iglesias-Suarez et al. (2020).

3.1. Evolution of Tropospheric Chemical Composition During the 21st Century

Figure 1 shows the temporal evolution of global mean surface abundance of O₃, NO_x, CH₄, CO + NMVOCs, hydrogen oxides (HO_x = HO₂+OH) and RO₂ (a generic peroxy radical not including HO₂), as well as the

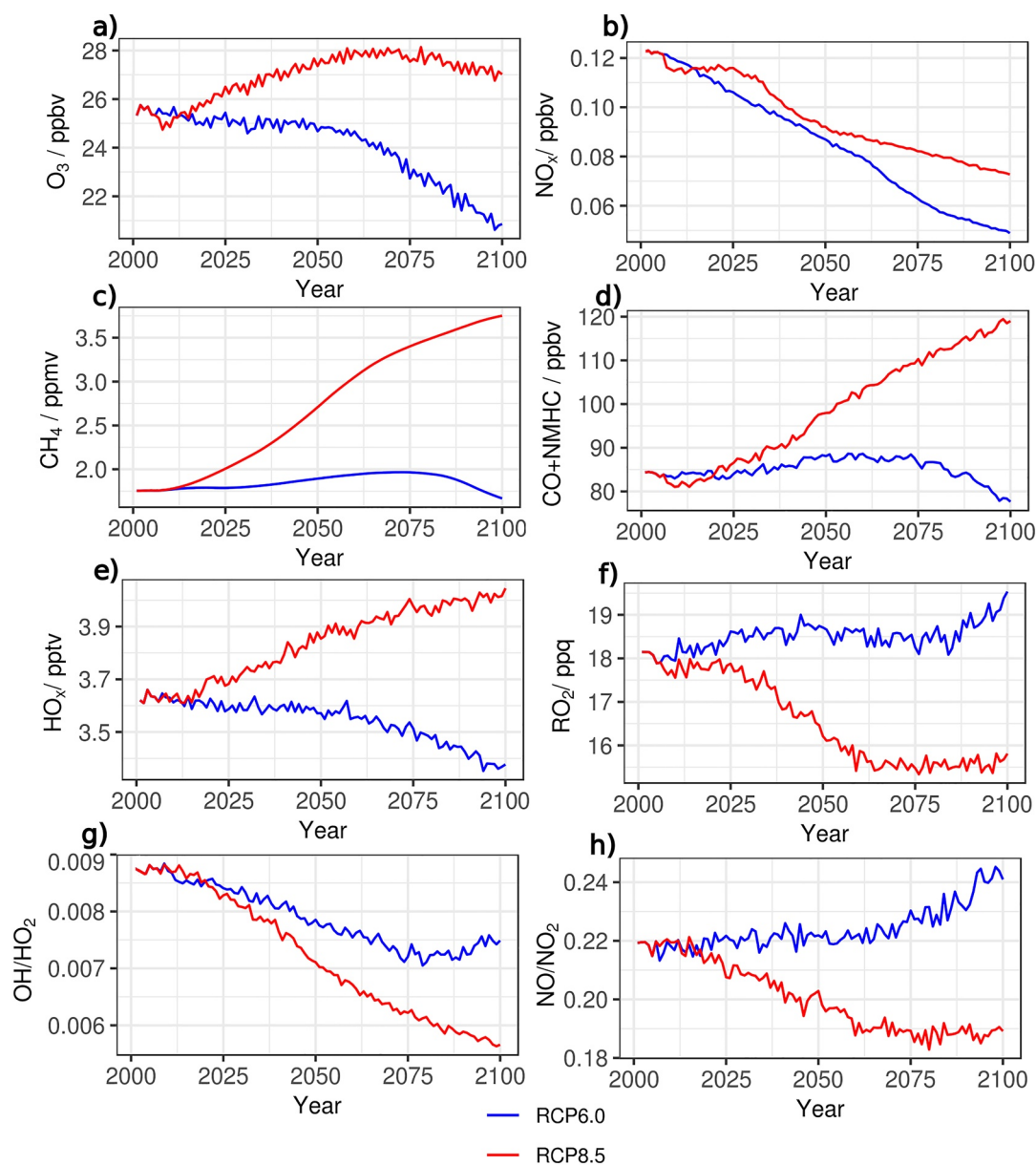


Figure 1. 21st century evolution of surface volume mixing ratios of O₃ (a), NO_x (b), CH₄ (c), CO + NMVOCs (d), HO_x (e) and RO₂ (f), as well as for the OH/HO₂ (g) and NO/NO₂ (h) ratio, for scenario Representative Concentration Pathway (RCP)6.0 (blue lines) and RCP8.5 (red lines).

OH/HO₂ and NO/NO₂ ratios over the 2000–2099 period. Under RCP6.0, O₃ decreases gradually until 2070 due to NO_x emission policy control. Concentrations of CH₄ are relatively constant (1–2 ppmv) during this period, presenting a small peak near year 2070, after which CH₄ drops to abundances smaller than those for year 2000 (along with CO + NMVOCs) that, together with the significant decrease in NO_x emissions, result in a rapid O₃ decrease toward the end of the century. It is worth noting that surface CO + NMHC abundances follow a similar trend to CH₄ (see Figures 1c and 1d). Consequently, an increase in the OH/HO₂ ratios after 2070 is observed as less hydrocarbons are available to react with OH (see Table S1 in Supporting Information S1). Oxidation of VOCs produces RO₂ intermediates that reacts with NO_x to produce O₃, and since less NO_x is available to react with RO₂ under RCP6.0, the concentration of peroxy radicals slightly increases, while ozone production decreases. In contrast, a very large increase of 4 ppmv in CH₄ (and CO + NMVOCs) is projected throughout the 21st century under RCP8.5, driving a global increase

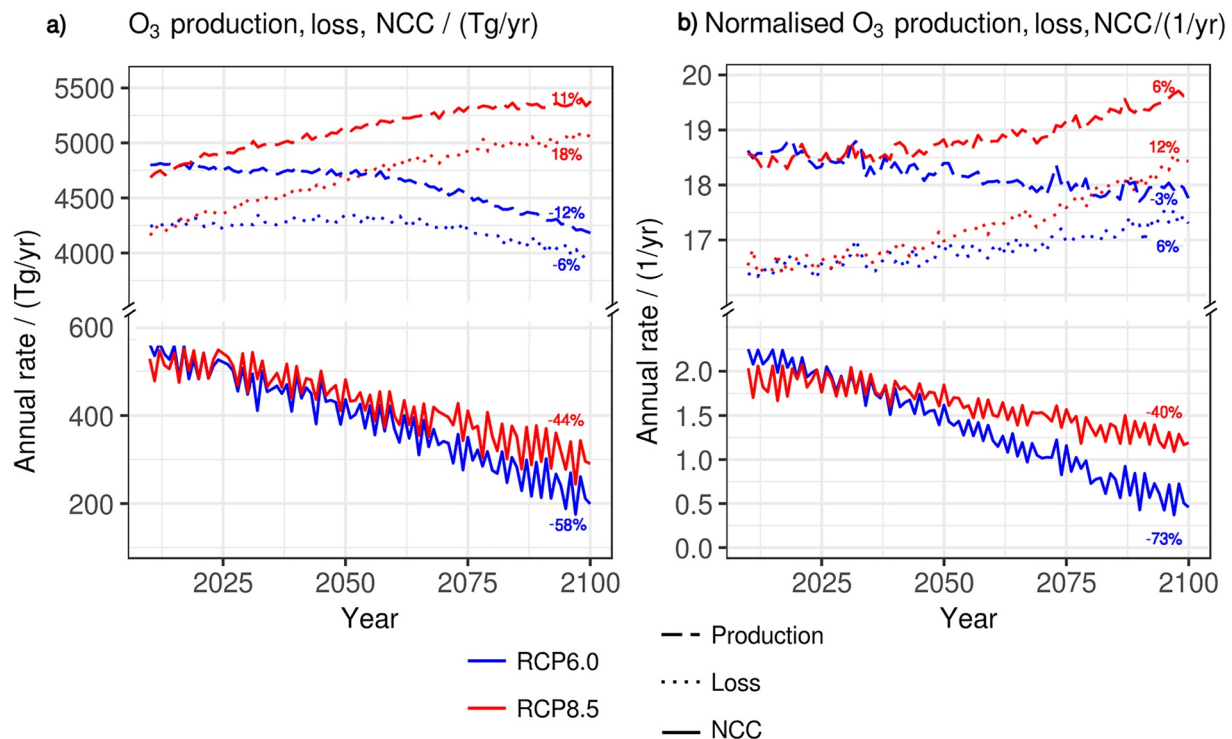


Figure 2. 21st century evolution of the total tropospheric ozone production, loss, and net chemical change (NCC) for scenario Representative Concentration Pathway (RCP)6.0 (blue lines) and RCP8.5 (red lines). Panel (a) shows absolute changes in Tg/year while panel (b) shows absolute changes normalized by the corresponding tropospheric ozone burden (1/year). Numbers above/below each line indicate the percentage of increase/decrease of each magnitude at the end of the century (2090–2099) with respect to the present-day (2000–2009).

in surface O_3 concentrations (up to 28 ppbv) until 2060–2070. After this decade, a slow-down in the CH_4 increase, coupled to a continuous reduction in NO_x , lead to the final O_3 reduction during the last quarter of the century. The oxidation of higher NMVOCs and CH_4 levels in RCP8.5 leads to much larger HO_2 (and to a smaller extent NO_2) compared to RCP6.0. As a result, a decrease of OH/HO_2 and NO/NO_2 ratios is predicted. Since more NO_x is available to react with RO_2 under RCP8.5, the peroxy radical concentration is lower than under RCP6.0.

3.2. Future Trends in Ozone Production, Loss, and NCC

Our results show that tropospheric NCC is projected to decrease significantly by the end of the century for both scenarios, especially in the case of RCP6.0 (−58%) (Figure 2). This is despite the different trends in ozone production and loss observed for RCP6.0 and RCP8.5. Compared to the present time, the relative decrease on ozone production by year 2100 within RCP6.0 (−565 ± 12 Tg/yr, −12 ± %) is proportionally larger than the decrease in ozone loss (−249 ± 3 Tg/yr, −6 ± 1%), resulting in a significant and continuous reduction of tropospheric NCC (−317 ± 16 Tg/yr, −58 ± 5%, see Figure 2a). Notably, when normalized by the annual ozone burden (Figure 2b), the gross O_3 production decreases (−3 ± 1%) while the ozone chemical loss increases (6 ± 2%), resulting in a significant reduction for the normalized NCC (−73 ± 10%). Even when the NCC trends for RCP8.5 show a similar trend, the production and loss terms present a completely different evolution: the increase in O_3 production (542 ± 17 Tg/yr, 113%)—which is driven by the future rise in methane and NMVOCs (Figure 1)—is surpassed by an even larger increase in O_3 losses (780 ± 4 Tg/yr, 18 ± 1%). Consequently, the RCP8.5 scenario leads to an absolute (−238 ± 26 Tg/yr, −44 ± 13%) and normalized (−40 ± 10%) tropospheric ozone NCC reduction. Overall, we find that when normalized to O_3 levels, there is a tendency throughout the 21st century to increase O_3 loss regardless of the emission scenario used in this study (see dotted lines in Figure 2b). Note that both scenarios lead to future global negative NCC since O_3 loss channels become more efficient than production pathways toward the end of the century (Figure 2). It

is worth highlighting that regardless of the emission scenario considered, very similar global production, loss and NCC trends are predicted at the surface level (Figure S2 in Supporting Information S1), although with a marked spatial and vertical variability within specific regions as described below.

Figure 3 indicates that, compared to the present-day, global NCC increases above 300 hPa ($\sim 2 \times 10^4$ molecules/cm³/s and $\sim 4 \times 10^4$ molecules/cm³/s following RCP6.0 and RCP8.5, respectively) and decreases below 300 hPa, particularly at the surface for RCP6.0 (-15×10^4 molecules/cm³/sec; see also Figure S3 in Supporting Information S1). The largest decrease is found in northern midlatitudes (30°N–60°N) for both scenarios, followed by the southern tropics (20°S–5°N) for RCP8.5 (Figures 3c and 3d). In contrast, positive surface NCC trends are projected over the northern subtropics (10°N–30°N) for RCP8.5. The magnitude and geographical pattern of normalized surface NCC evolution also differ between the two scenarios (Figures 3e and 3f). For RCP6.0, the largest decrease is projected at midlatitudes in both hemispheres from 2070 until the end of the century (Figure 3e), whereas for RCP8.5 normalized NCC decreases in the tropical boundary layer and increases in the northern extratropics, mostly during the first half of the century (Figure 3f). Overall, these results indicate that even when the global ozone tropospheric NCC is projected to decrease regardless of the scenario considered, a marked geographical and vertical variability is to be expected in the future evolution of ozone chemistry.

3.3. Vertical and Spatial Evolution of the Dominant Chemical Drivers

The modeled surface HO₂ + NO production pathway decreases everywhere, with a particularly significant decline over midlatitudes within RCP6.0 (up to 72% in the Northern Hemisphere [NH] extratropics). This is related to the large reduction in O₃ precursor emissions (NO_x, CO + NMHC, CH₄) that reduces HO₂ and NO levels (Figure 1), which in turn reduces also the O₃ production via RO₂ + NO from the surface to the middle troposphere (Figures 4a–4c, 5a and 5b). Under RCP8.5, a different pattern is observed for production via RO₂ + NO. Note that the global temperature rise under climate change enhances CH₄ oxidation by OH (the reaction has a positive activation energy which leads to an acceleration of the reaction at higher temperatures) (Atkinson, 2003) which increases methylperoxy radical (CH₃O₂) production mostly in the upper troposphere. Thus, following the significant increase in CH₄ emissions and temperature under RCP8.5, O₃ production increases by 52% through RO₂ + NO primarily via CH₃O₂ + NO which competes with the dominant HO₂ + NO channel—which, in turn, is projected to decrease in the lower troposphere mostly within the NH (Figures 4d–4f, 5e and 5f). O₃ production mediated by the RO₂ + NO reaction increases globally but more markedly over the NH tropics (0°–30°N) under RCP8.5, being highest over the surface of western Africa, South America, India and southeast Asia (Figure 6). Our results show that the globally integrated change in O₃ production throughout the century is dominated by changes in precursor emissions in the NH. The results of this study are in agreement with previous studies that indicate that O₃ production over the tropical middle and upper troposphere, mainly driven by increasing lightning-NO_x emissions as well as other O₃ precursors, can be efficiently transported to upper levels due to enhanced atmospheric convection under climate change (Finney et al., 2016; Iglesias-Suarez et al., 2018). We now turn to the modeled changes in the main chemical ozone destruction channels (oxygen-catalyzed (Ox_{loss}), hydrogen-catalyzed (HOx_{loss}) and halogen-mediated (Halogens_{loss}) cycles, defined in Section 2). In general, future versus present-day differences under RCP6.0 are more pronounced in the NH than in the Southern Hemisphere (SH) (Table 1 and Figure 7), where the influence of anthropogenic emissions is smaller throughout the century. For the NH, negative O₃ loss trends (up to -16×10^4 molecules/cm³/s) occur primarily via Ox_{loss} and HOx_{loss} especially at the surface within extratropical industrialized regions, such as the eastern United States, Europe and eastern Asia (Figures 7a, 8 and 9). Here, the lower tropospheric O₃ abundances projected after 2070 drive a pronounced reduction of the HO₂ + O₃ (–42%) and OH+O₃ (–38%) loss channels mostly during the second half of the century. Note that the projected decline in inorganic iodine emissions in RCP6.0 (Iglesias-Suarez et al., 2020) (Figure S4a in Supporting Information S1) is mostly driven by the decrease of surface O₃ levels since the main global iodine emission source arises from the deposition of O₃ to the surface ocean and subsequent reaction with iodide (I[–]) (Carpenter et al., 2013). The decline in iodine emissions and in tropospheric O₃ levels in RCP6.0 decreases Halogens_{loss} cycles up to -2×10^4 molecules/cm³/s over the NH (Figure 7a). On the other hand, an enhanced surface ozone gross chemical destruction of up to 8×10^4 molecules/cm³/s is modeled globally for RCP8.5 (Figure 7f), which is mainly driven by the net increase in surface O₃ mixing ratios (see Figure 1a). This chemical loss enhancement is particularly high over Africa, India and Australia

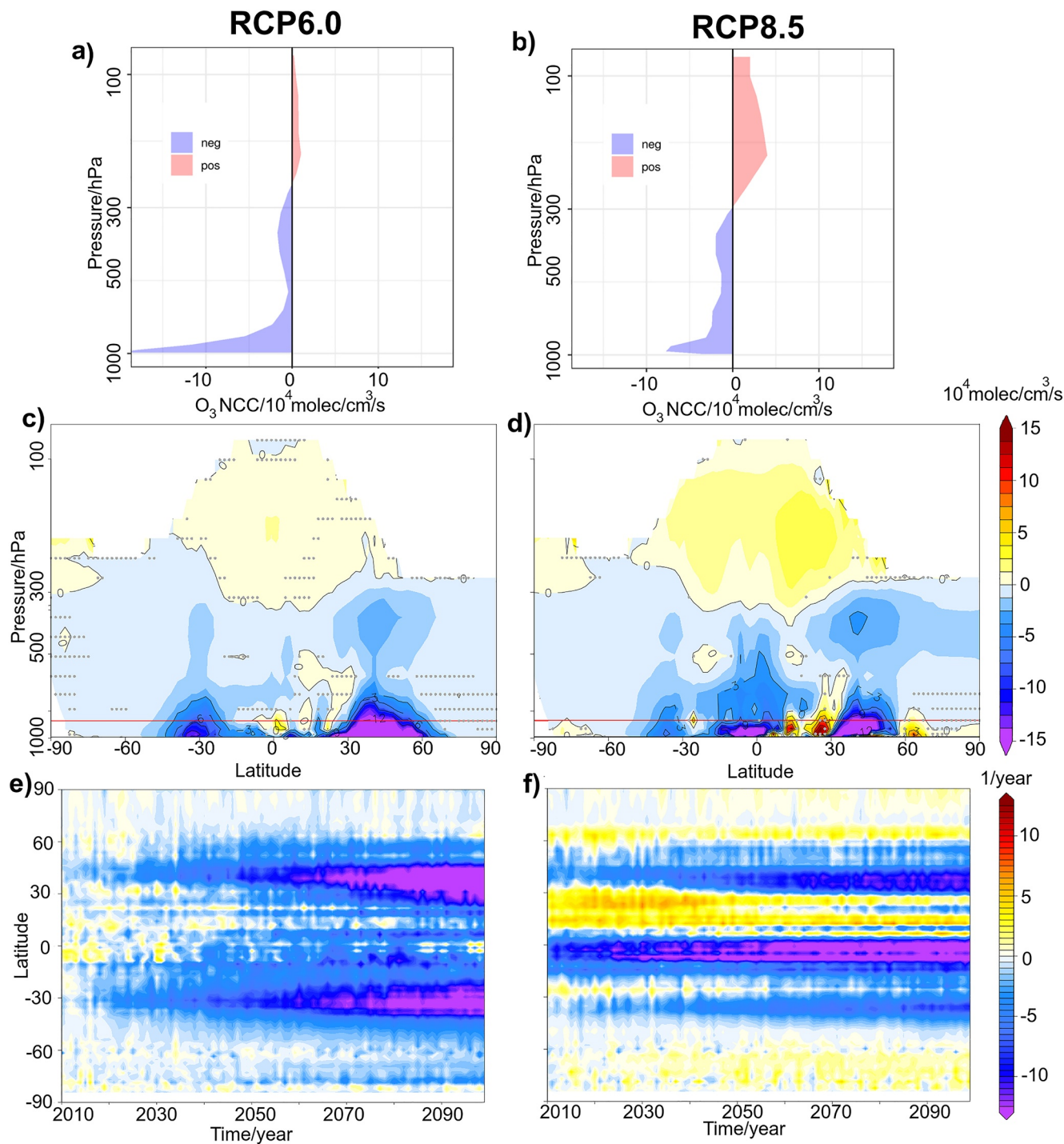


Figure 3. Vertical (a and b) and zonal (c and d) net chemical change (NCC) between the end of the century (2090–2099) and present-day (2000–2009) for scenario Representative Concentration Pathway (RCP)6.0 (left panels) and RCP8.5 (right panels). Panels (a–d) show absolute changes in $10^4 \text{ molecules/cm}^3/\text{sec}$. Panels (e and f) show the surface (lower model levels with pressure >850 hPa). NCC latitudinal mean evolution normalized by O_3 abundance (1/year). Hatching indicates trends are not significant at the 95% confidence interval (two-sigma of the standard error trend). Horizontal red line in panels (c and d) shows the 850 hPa pressure.

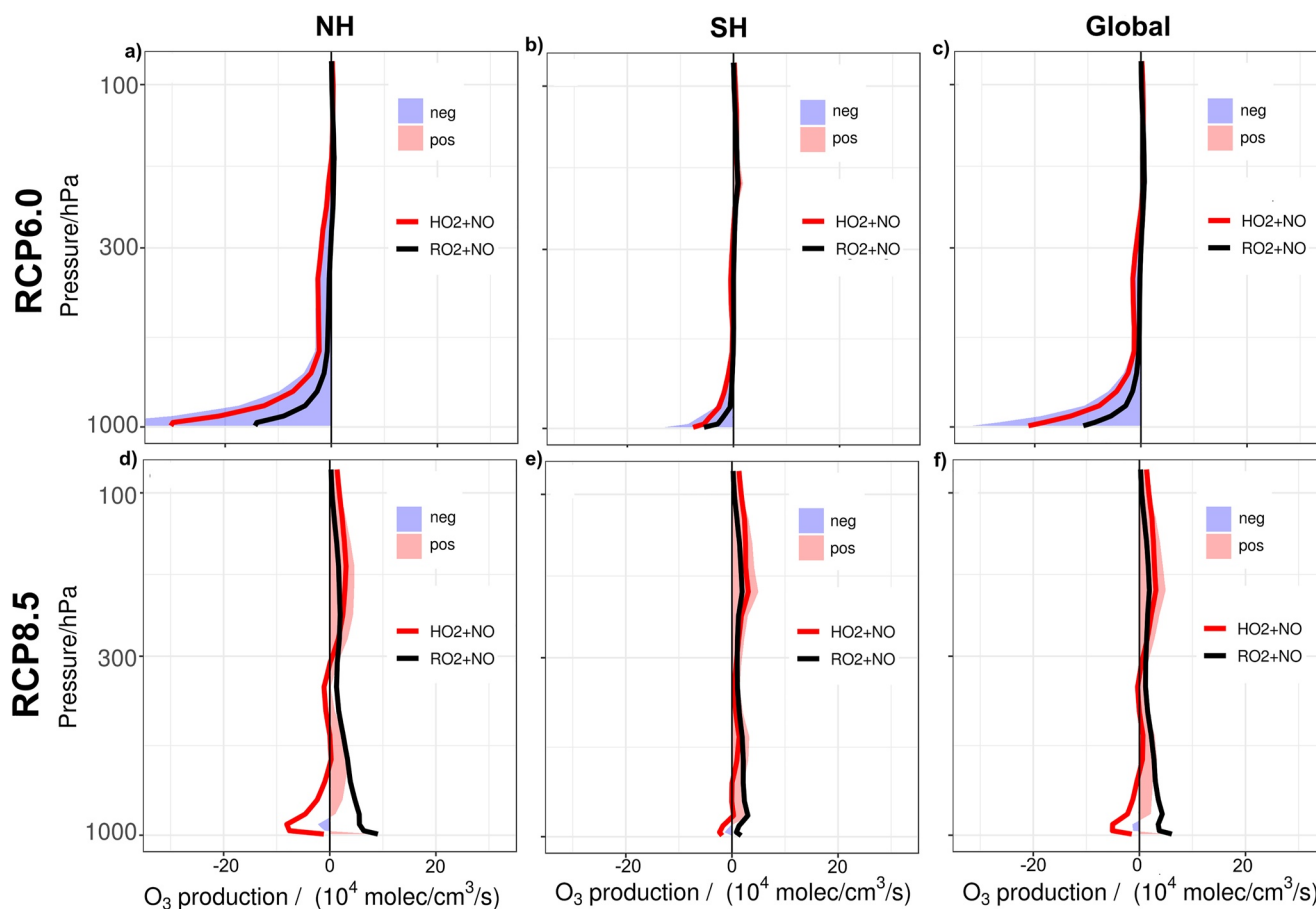


Figure 4. Change in ozone chemical production between the end of the century (2090–2099) and present-day (2000–2009) under Representative Concentration Pathway (RCP)6.0 (a–c) and RCP8.5 (d–f) scenarios. Only the main production channels ($\text{HO}_2 + \text{NO}$ and $\text{RO}_2 + \text{NO}$) are considered. Panels (a and d) are for the Northern Hemisphere (NH), panels (b and e) for the Southern Hemisphere (SH), and panels (c and f) for the Global mean (see text for details). Units are in 10^4 molecules/ cm^3/sec . Red shaded areas show future production enhancements (pos) while blue shaded areas indicate the chemical production decreases (neg).

(Figures 8 and 9) due to: (a), a significant increase in the water vapor mediated O_3 loss—via $\text{O}(^1\text{D})+\text{H}_2\text{O}$ —in the tropical lower to middle troposphere mostly during the second half of the century (Figures 8g and 8j) due to the global warming-driven evapotranspiration from the oceans; (b), an increase in CH_4 concentration that changes the OH/HO_2 ratio (Figure 1g) resulting in more efficient HOx_{loss} cycles within the NH midlatitudes (Figure 8h); and (c) an increase in inorganic iodine emissions (Figure S4b in Supporting Information S1) that accelerates $\text{Halogen}_{\text{loss}}$ cycles, mostly close to the surface (Figure 8i). Due to its larger ozone-depleting efficiency, compared to bromine and chlorine, iodine is the main halogen-mediated ozone loss chemistry (Figure S5 in Supporting Information S1), especially in the MBL (Badia et al., 2019; Cuevas et al., 2018; Mahajan et al., 2021; Saiz-Lopez et al., 2014). Further details on the chemistry behind the influence of halogens on the OH/HO_2 and NO/NO_2 ratios in the MBL is provided elsewhere (Read et al., 2008; Saiz-Lopez & von Glasow, 2012; Saiz-Lopez et al., 2014).

As previously noted, normalized surface O_3 loss is projected to increase under both scenarios by the end of this century. However, when split by family, we find that losses through Ox_{loss} and $\text{Halogen}_{\text{loss}}$ cycles are the main drivers of the future O_3 loss enhancement (especially between 2070 and 2099), while surface HOx_{loss} show a slight reduction moving toward the end of the century (Figures 8d–8f and 8j–l).

3.4. Regional Variability

We find that the evolution of O_3 chemistry in a future climate is complex, regionally varying and strongly influenced by changes in emissions and atmospheric dynamics. Figures 10 and 11 show changes in surface

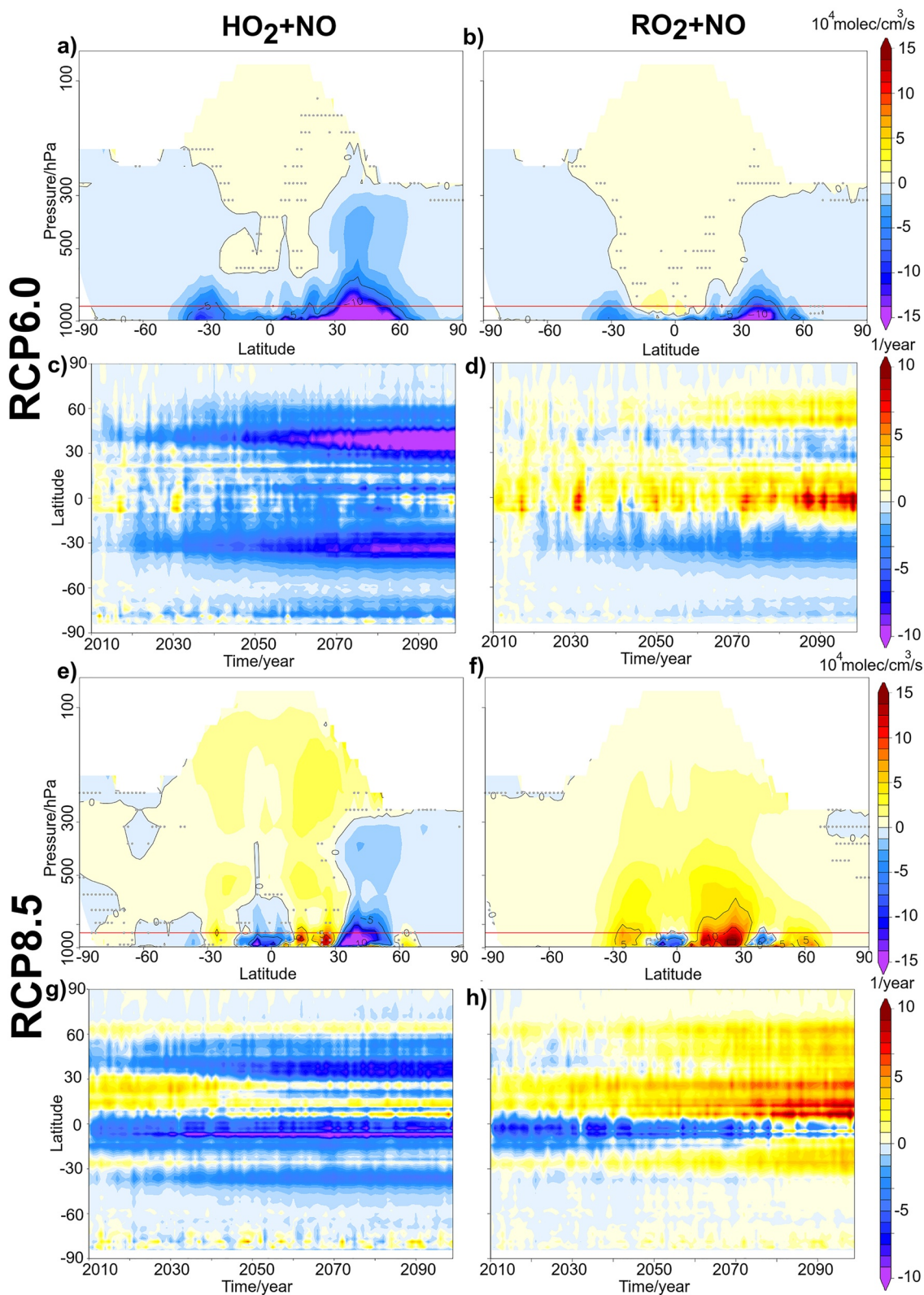


Figure 5. Zonal changes in chemical production between the end of the century (2090–2099) and present-day (2000–2009). Only the main production channels ($\text{HO}_2 + \text{NO}$ and $\text{RO}_2 + \text{NO}$) are considered. Panels (a, b, e, f) show absolute changes in 10^4 molecules/ cm^3/sec . Panels (c, d, g, h) show averages on the surface level normalized by O_3 concentrations (units are 1/year). Hatching indicates trends are not significant at the 95% confidence interval (two-sigma of the standard error trend). Horizontal red line in panels (a, b, e, f) show the 850 hPa boundary for the surface.

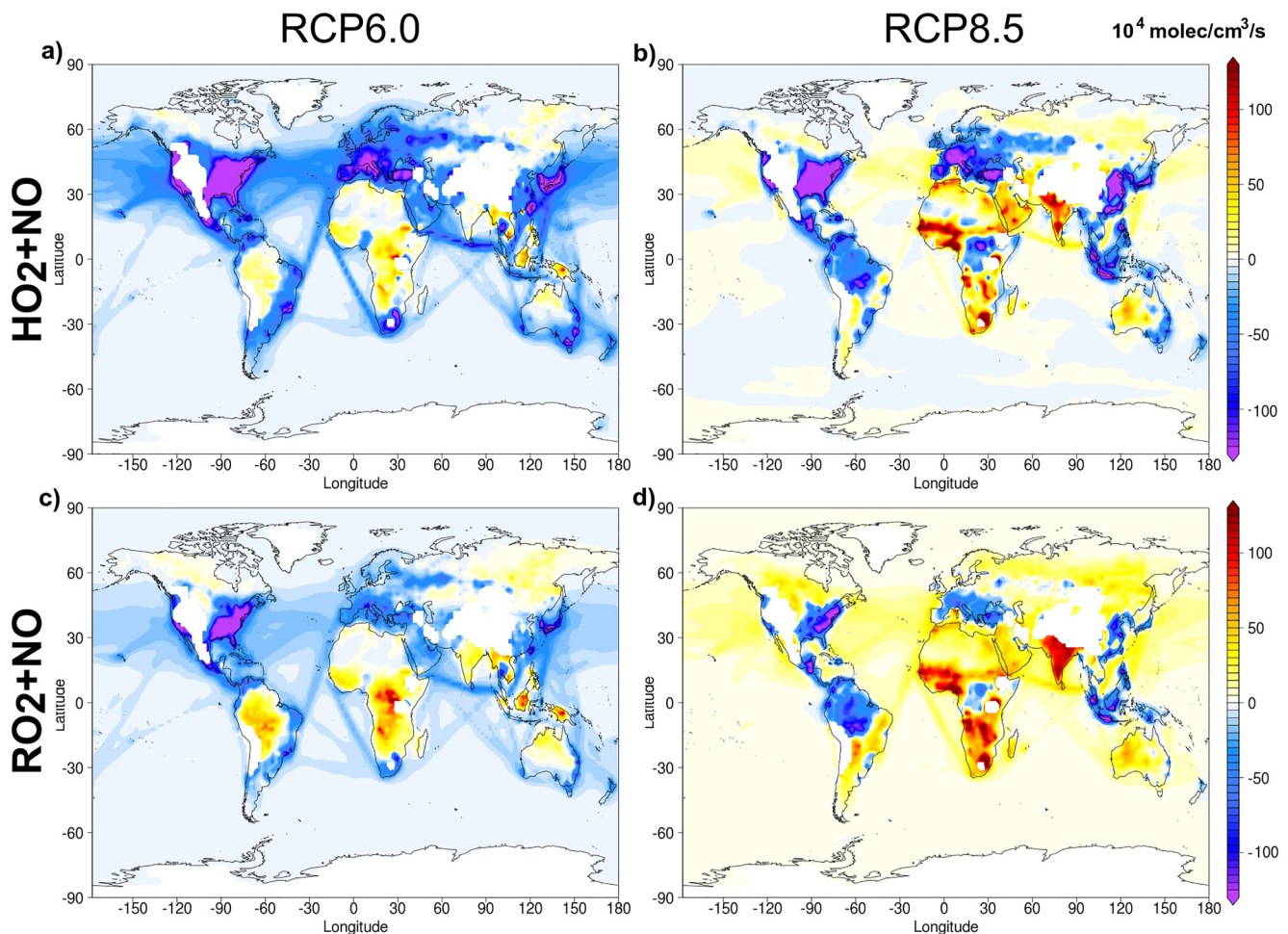


Figure 6. Regional changes of the surface ozone chemical production between the end of the century (2090–2099) and present-day (2000–2009) under Representative Concentration Pathway (RCP)6.0 (a and c) and RCP8.5 (b and d). Only the main production channels ($\text{HO}_2 + \text{NO}$ and $\text{RO}_2 + \text{NO}$) are considered. Units are in 10^4 molecules/ cm^3/sec . Surface values refer to lower model levels with pressure >850 hPa.

NCC and O_3 concentrations, respectively. NCC decreases markedly ($\sim -150 \times 10^4$ molecules/ cm^3/s , $\sim -60\%$, for RCP6.0) over industrialized regions in the NH (eastern United States and regions of Europe and eastern Asia, Figures 6a and 6c) due to stringent reductions in precursor emissions (mostly CO and NO). In contrast, we predict large NCC increases ($100\text{--}150 \times 10^4$ molecules/ cm^3/s , 50 to 150%) over Africa, India, and Australia are due to enhanced O_3 production efficiency (Figures 6b and 6d), which is explained by the greater projected precursor emissions (CO, C_2H_6 , and NO) especially under RCP8.5 (Figure 6). Note that in the marine atmosphere, NCC is strongly linked to both natural halogens emitted from the oceans and emissions from the shipping industry because even though reactive halogens destroy O_3 via combined catalytic $\text{BrOx}_{\text{loss}} - \text{ClOx}_{\text{loss}} - \text{IOx}_{\text{loss}}$ cycles, shipping emissions lead to O_3 production (Eyring et al., 2010; Li et al., 2021). Notably, a significant decrease in ozone NCC is projected over marine midlatitudes along the main shipping tracks under RCP6.0. In contrast, for the RCP8.5 simulations we model a marked hemispheric difference with slightly positive trends in surface NCC for the NH and a predominantly oceanic negative NCC evolution in the SH (Figure 10).

Over the continents, there is a spatial correlation between NCC and O_3 concentration changes over most locations (see Figures 10 and 11), in particular over the eastern United States and industrialized regions of Europe and Asia, where surface O_3 reductions range between 5 to 25 ppbv (10–30%). However, there are continental regions where this spatial correlation is not observed. For example, in some areas over South America and North Africa, future O_3 concentrations are projected to decrease (~ -10 ppb, $\sim -15\%$) under

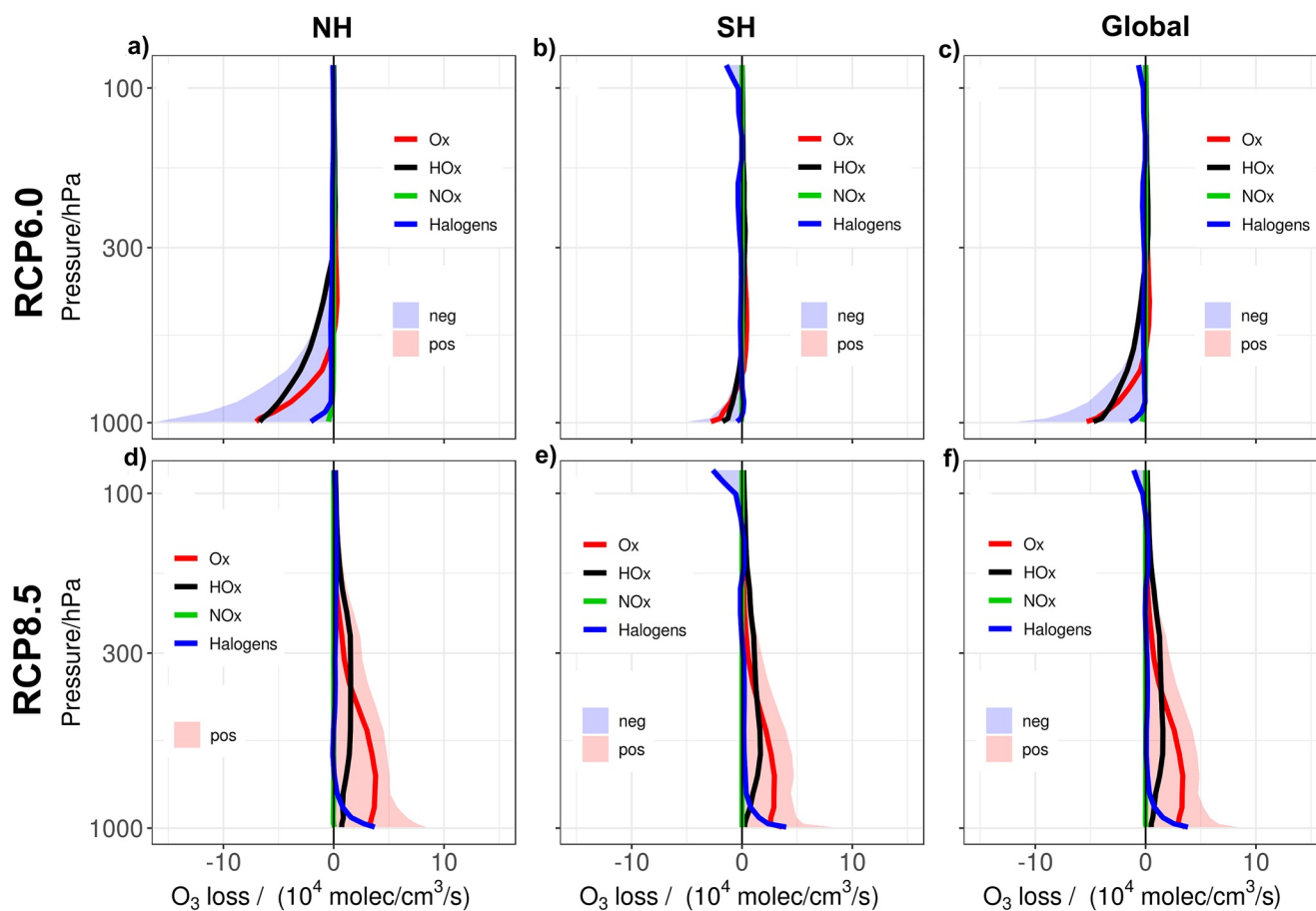


Figure 7. Change in ozone chemical loss between the end of the century (2090–2099) and present-day (2000–2009) under Representative Concentration Pathway (RCP)6.0 (a–c) and RCP8.5 (d–f) scenarios. Only the main loss cycles (HOx_{loss} , Ox_{loss} , NOx_{loss} , and $\text{Halogens}_{\text{loss}}$) are considered (see text for details). Panels (a and d) are for the Northern Hemisphere (NH), panels (b and e) for the Southern Hemisphere (SH), and panels (c and f) for the Global mean. Units are in 10^4 molecules/cm³/sec. Red shaded areas show future loss enhancements (pos) while blue shaded areas indicate the chemical loss decreases (neg).

RCP6.0 even when NCC increases (Figures 10b, 10d, and 11d). Similarly, over Western Europe and Eastern Australia, future O_3 levels increase under RCP8.5 (~5 ppb, ~6%) while NCC decreases. Differences between NCC and O_3 concentrations are mainly related to tropospheric transport changes (horizontal transport and downward subsidence from the stratosphere), as well as to trends in other atmospheric processes such as trace gases removal by dry and wet deposition. In addition, contrasting hemispheric trends are also appreciable over the ocean, where O_3 concentrations under RCP6.0 decrease (up to 15 ppb, 30% over the NH), and slightly increase (5 ppb) under RCP8.5, with significant changes over the SH (30%) (Figure 11). Note that future O_3 levels under RCP8.5 decrease over the Eastern Pacific and the Mediterranean, associated with the outflow of continental low O_3 air masses (Archibald, Turnock, et al., 2020).

We now evaluate the percentage change evolution of the main chemical production and loss channels at the surface for different regions during the 21st century, relative to the present-day (Figure 12). In terms of O_3 production, both scenarios show similar trends (albeit differences in magnitude) presenting a shift from a dominant hydrogen-driven ozone formation to a comparatively more important peroxy radical-driven O_3 production as we move into the future. Globally, surface $\text{RO}_2 + \text{NO}$ increases by up to 6% and $\text{HO}_2 + \text{NO}$ decreases 6% by the end of this century, with the highest changes over the southeastern United States (up to $\pm 12\%$) due to the significant decline in projected anthropogenic emissions in that region. Surface Halogen- s_{loss} cycles (mainly iodine, Figure S6 in Supporting Information S1) are projected to become more efficient under both scenarios (2–3% globally), especially over coastal regions such as Europe-Mediterranean (3%), and South East Asia (3–5%). By the end of the century, Ox_{loss} cycles also become slightly more efficient (1.5% globally), with the greatest enhancement over the tropics (3–5%) driven by higher atmospheric water vapor

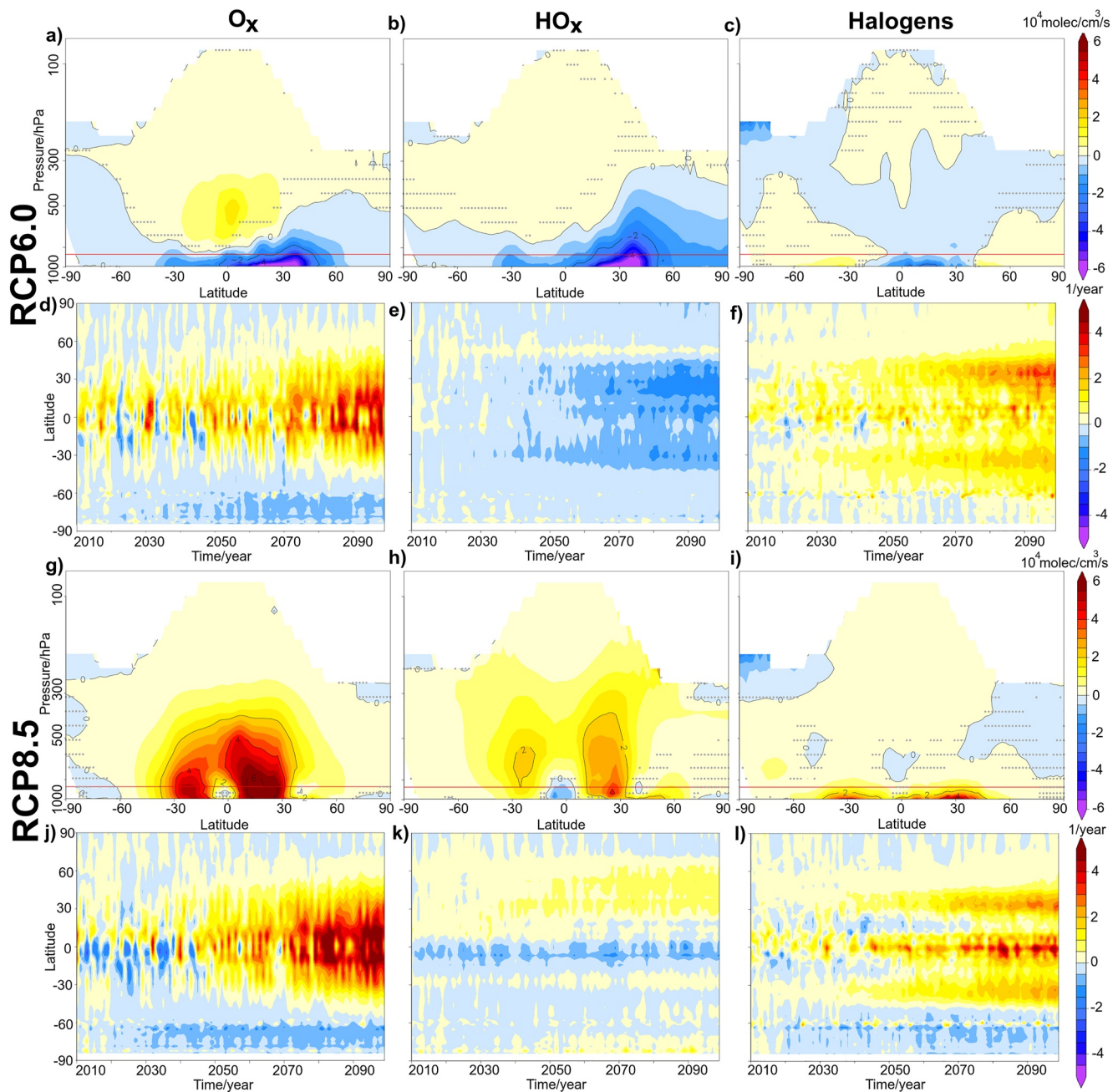


Figure 8. Zonal changes in chemical loss between the end of the century (2090–2099) and present-day (2000–2009). Only the main loss cycles (HOx_{loss} , Ox_{loss} , and $\text{Halogens}_{\text{loss}}$) are considered. Panels (a–c and g–i) show absolute changes in 10^4 molecules/ cm^3/sec and the horizontal red line show the surface level. Panels (d–f and j–l) show averages on the surface level by O_3 levels (units are 1/year). Hatching indicates trends are not significant at the 95% confidence interval (two-sigma of the standard error trend). Horizontal red line in panels (a–c and g–i) show the 850 hPa boundary for the surface.

due to global warming (Figure S7 in Supporting Information S1). As a consequence, the dominant HOx_{loss} cycles are projected to decrease in magnitude as the century progresses (-4% under RCP6.0 and -2% under RCP8.5) which is compensated by Ox_{loss} and $\text{Halogens}_{\text{loss}}$ enhancement (Figure 12). Overall, and although the future ozone production and losses trends are significantly different between RCP6.0 and RCP8.5, the change in relative efficiency for each chemical channel will be globally similar for both scenarios throughout the century. Notably, the future evolution of $\text{Halogens}_{\text{loss}}$ cycles, along with the RO_2+NO production term (which is also affected by the presence of natural halogens), are predicted to be the chemical channels with the largest percentage change (Figure 12), highlighting the importance of considering natural halogen

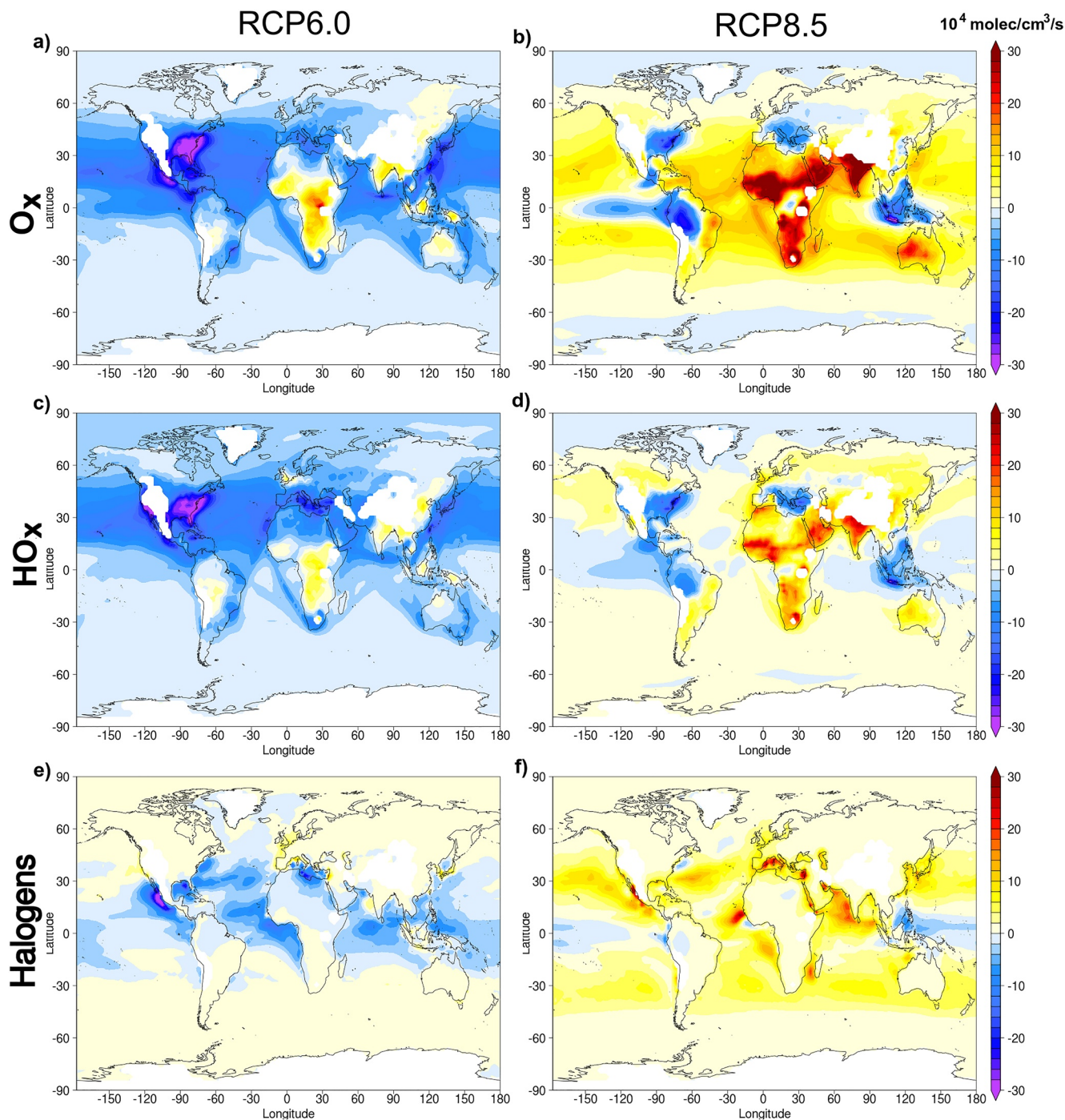


Figure 9. Regional changes of the surface ozone chemical loss between the end of the century (2090–2099) and present-day (2000–2009) under Representative Concentration Pathway (RCP)6.0 (a, c, e) and RCP8.5 (b, d, f). Only the main loss cycles (HOx_{loss} , Ox_{loss} , and $\text{Halogens}_{\text{loss}}$ cycles) are considered. Units are in 10^4 molecules/ cm^3/sec . Surface values refer to lower model levels with pressure >850 hPa.

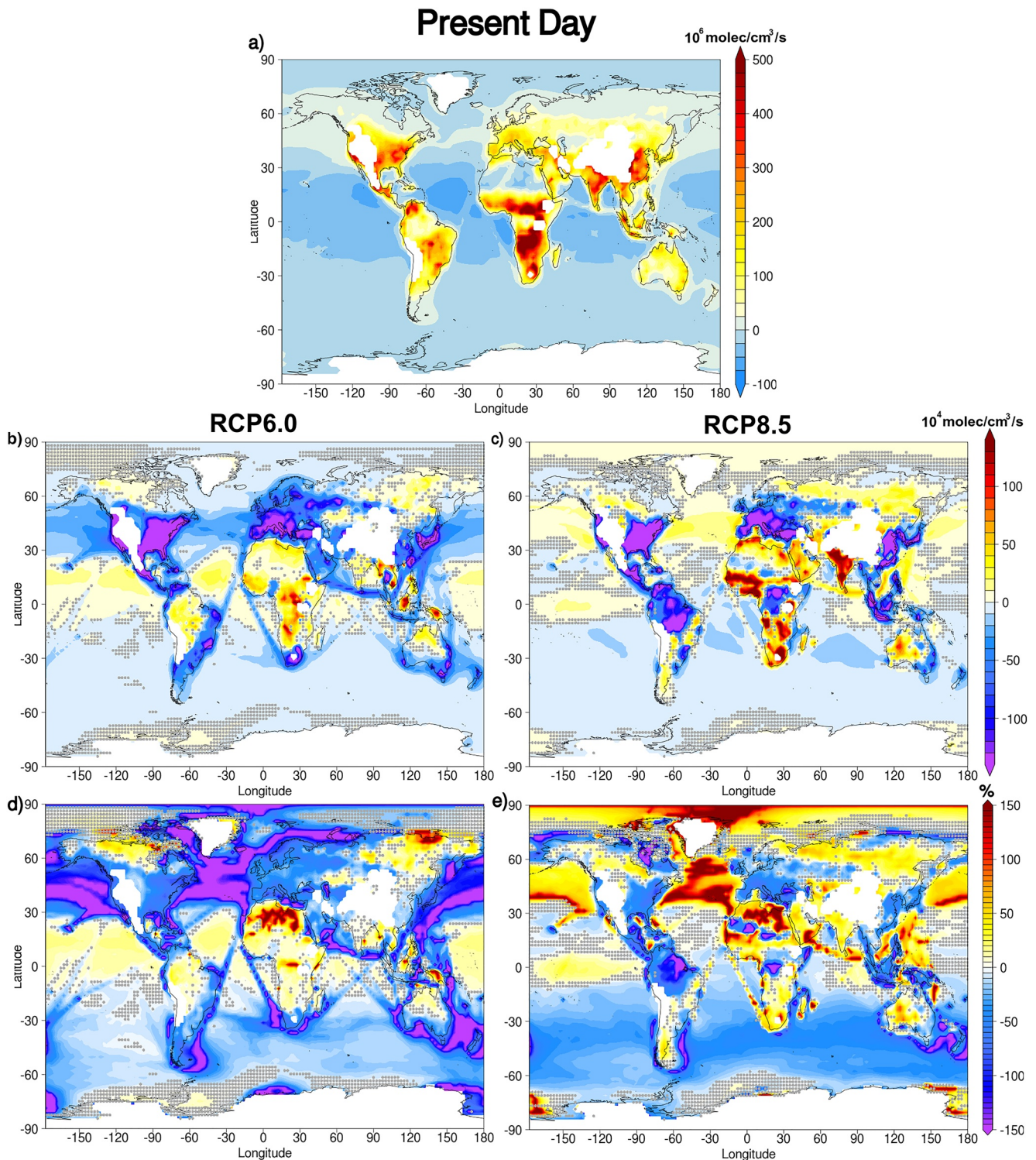


Figure 10. Spatial distribution of present-day surface net chemical change (NCC) (a), as well as its regional changes between the end of the century (2090–2099) and present-day (2000–2009) under Representative Concentration Pathway (RCP)6.0 (b) and RCP8.5 (c). Note that present-day NCC is scaled by 10^6 molecules/ cm^3/s , while NCC changes are scaled by 10^4 molecules/ cm^3/s . Panels (d and e) show the corresponding percentage NCC change with respect to present-day. Hatching indicates trends are not significant at the 95% confidence interval (two-sigma of the standard error trend). Surface values refer to lower model levels with pressure >850 hPa.

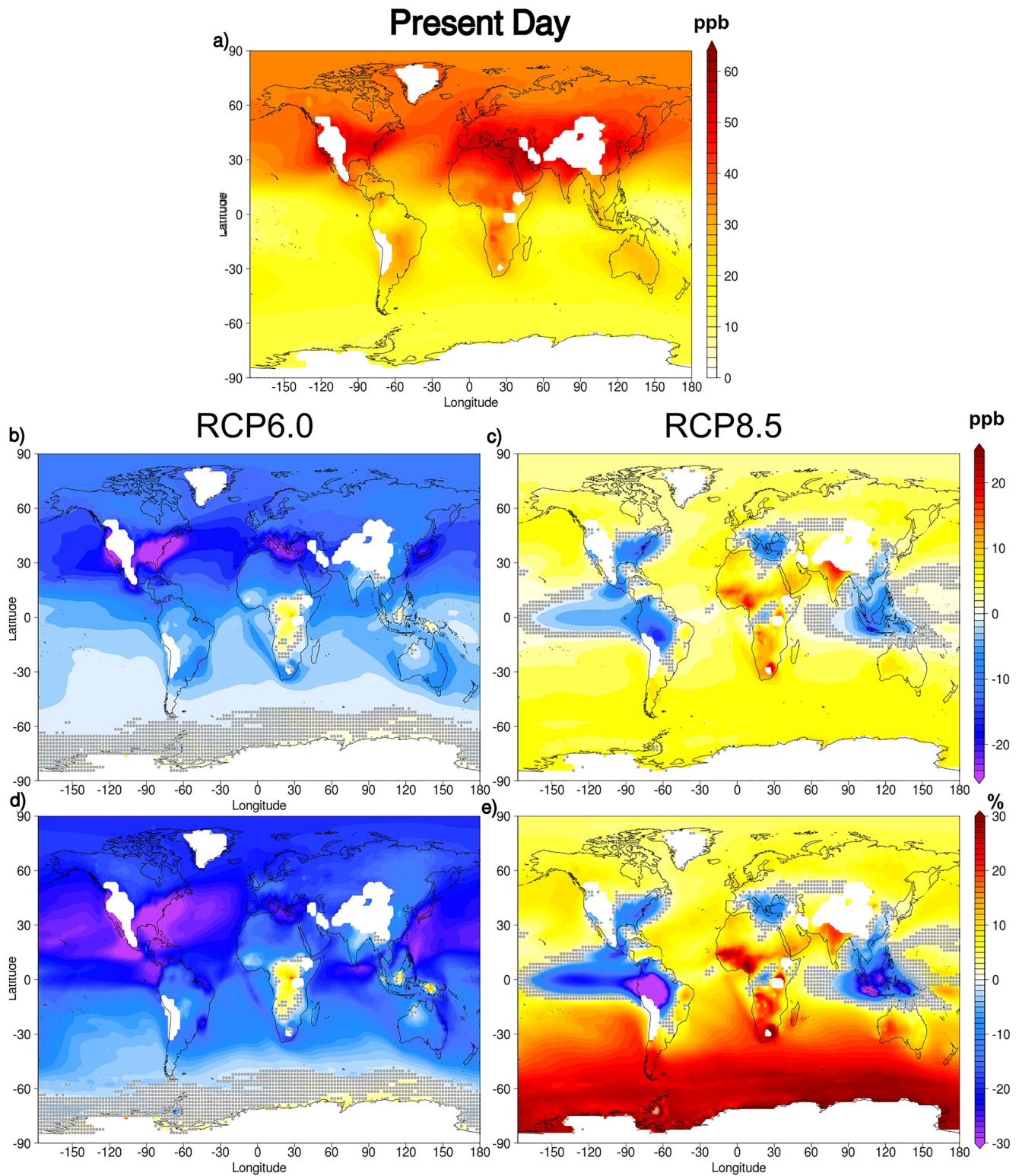


Figure 11. Spatial distribution of the present day surface O₃ volume mixing ratio (a), as well as its regional changes between the end of the century (2090–2099) and present-day (2000–2009) under Representative Concentration Pathway (RCP)6.0 (b) and RCP8.5 (c). Absolute changes are expressed in ppbv (a–c). Panels (d and e) show the corresponding percentage change. Hatching indicates trends are not significant at the 95% confidence interval (two-sigma of the standard error trend). Surface values refer to lower model levels with pressure >850 hPa.

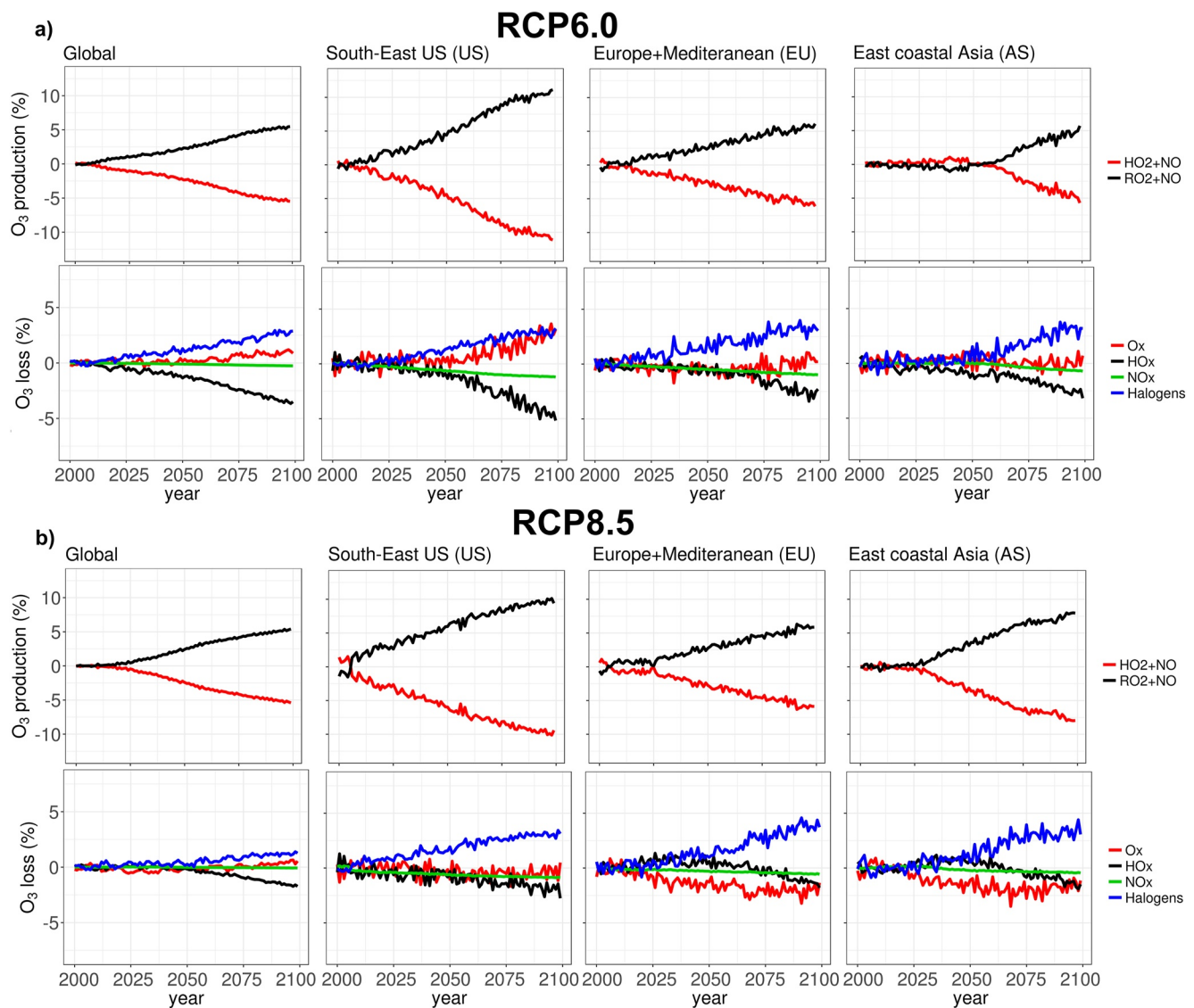


Figure 12. 21st century evolution of the normalized surface ozone production and loss terms under Representative Concentration Pathway (RCP)6.0 (a) and RCP8.5 (b) for different regions. Each row presents the O_3 production (top) and loss (bottom) within each scenario, while each column indicates a specific region: global, South-East United States (95°W – 75°W and 30°N – 45°N), Europe and the Mediterranean Sea (10°W – 36°W and 30°N – 55°N), and East Coastal Asia (90°E – 150°E and 10°S – 10°N).

sources and chemistry within chemistry-climate projections. Equivalent results for whole troposphere are shown in Figure S8 in Supporting Information S1.

3.5. Comparing Present-Day and Future Ozone Budgets

Table 1 summarizes the present-day and the end of the century tropospheric O_3 budget under RCP6.0 and RCP8.5. Equivalent results for the surface O_3 budget are reported in Table S2 in Supporting Information S1. Present-day chemical production (4,792 Tg/yr) is dominated by HO_2+NO (3,006 Tg/yr), while chemical losses (4,250 Tg/yr) are driven by Ox_{loss} (1,991 Tg/yr), HOx_{loss} (1,468 Tg/yr), and halogens (649 Tg/yr). The present-day tropospheric ozone NCC derived from these terms is 542 Tg/yr. According to our calculations, 873 Tg of O_3 are currently removed from the troposphere by dry deposition (475 Tg over land and 334 Tg over water, see Table 2), while the modeled STT reaches 331 Tg/yr. The modeled dry deposition value is in line

Table 2
Changes in O₃ Deposition During the 21st Century

Dry deposition (D)	Land type	Present-day	Future (RCP6.0)	Future (RCP8.5)
D(O ₃)	Land	475	395 (−17%)	446 (−6%)
	Water	334	266 (−20%)	335 (0%)
	All	809	661 (−18%)	781 (−3%)
D(IO _y)	Land	0.0	0.0	0.0
	Water	0.45	0.5 (10%)	0.6 (28%)
	All	0.45	0.5 (10%)	0.6 (28%)
D(NO _y)	Land	38	22 (−42%)	23 (−39%)
	Water	24	10 (−58%)	14 (−42%)
	All	63	32 (−51%)	37 (−41%)
Total	Land	513	417 (−19%)	469 (−9%)
	Water	359	276 (−23%)	350 (−3%)
	All	872	694 (−21%)	819 (−6%)

Note. Units are in Tg/yr. The percentage of increase/decrease by the end of the century (2090–2099) respect to the present-day (2000–2009) is shown in parentheses for each term. See Lamarque et al. (2012) and Section 2 for further details on the definition of species. RCP, Representative Concentration Pathway.

with a recent study that reports a range of 815–907 Tg/yr removed by dry deposition over 2005–2014 in the CMIP6 models (Griffiths et al., 2021).

The calculation of the ozone burden is uncertain and is sensitive to the tropopause definition used (Archibald, Neu, et al., 2020; Griffiths et al., 2021; Wild, 2007). Previous studies have used the chemical tropopause at the 150 ppbv contour of O₃ (Stevenson et al., 2006; Young et al., 2013) for their calculation of the ozone burden, however, other studies suggest to use a lower definition, 125 ppbv, to have less stratospheric influence (Archibald, Neu, et al., 2020; Prather et al., 2011). Here we use three different definitions for the tropopause to calculate our modeled ozone burden. The resulting present-day total tropospheric burden obtained including natural halogen chemistry is 293 Tg (261 Tg between 60°S–60°N), 280 Tg (250 Tg between 60°S–60°N) and 317 Tg (281 Tg between 60°S–60°N) using the chemical tropopause at the 150 ppbv contour of O₃, at 125 ppbv contour of O₃ and the modeled WMO tropopause (Reichler et al., 2003) definition, respectively. These results lie within the lower range of satellite estimates of the present-day tropospheric burden (~250–325 between 60°S and 60°N) (see Gaudel et al., 2018; Griffiths et al., 2021) and are about 15% lower than the ozonesonde-based TOST calculated global burden (344 Tg for the 150 ppbv ozone tropopause, 328 Tg for 125 ppbv ozone tropopause and 369 Tg for the lapse rate tropopause definitions). However, ozonesondes apparently measure about 5% high in the troposphere on average, compared to IAGOS aircraft and other UV-absorption methods (Tarasick et al., 2019). Although our modeled present-day O₃ lifetime (τ_{O_3}), 20.9 days, is lower than the mean

CMIP6 estimated range (25.5 ± 2.2 days), our simulations account for the ozone loss due to tropospheric natural halogens that can decrease the O₃ lifetime 2 days (Iglesias-Suarez et al., 2020). Indeed, our estimated lifetime for the NONATHAL simulation during present time reaches 23 days.

The future tropospheric O₃ budget shows significant differences between the two scenarios, which can be explained by the production and loss trends described in previous sections. For example, the chemical production (−12%) decreases following RCP6.0 are mainly driven by the change in the HO₂+NO reaction channel (−15%). By contrast, chemical production in RCP8.5 increases substantially (11%), driven by changes in RO₂+NO (26%), which results from the increase in peroxy-radicals arising from the breakdown of CH₄ and other NMVOCs. The chemical loss also shows opposite trends between scenarios with a reduction under RCP6.0 (−6%) and an increment under RCP8.5 (18%). For RCP6.0, the reduction is mainly driven by HO_x loss (−10%) and Halogens_{loss} cycles (−7%). On the other side, the predicted increase of O_x loss (21%), HO_x loss (16%) and Halogens_{loss} (9%) loss cycles under RCP8.5 is due to higher water vapor, increased HO₂ levels, and anthropogenically enhanced ocean halogen emissions (mostly iodine), respectively. Changes in the tropospheric aerosol burden (in particular on the aerosol surface area density) can shift NO_x/NO_y (where NO_y is defined as the total reactive nitrogen compounds) and HO_x/H₂O₂ (H₂O₂, the hydrogen peroxide) ratios following the heterogeneous reactivation of halogen, nitrogen and hydrogen reservoirs (Saiz-Lopez & von Glasow, 2012). These changes can enhance the OH concentration, thereby impacting on the methane lifetime (Tilmes et al., 2015). However, future changes in the aerosol burden are not expected to directly impact on the ozone burden, as O₃ loss via aerosols—included in the other O_x loss term (Table 1)—only accounts for less than 1% with respect to the total O₃ loss. Based on this analysis, we project a global tropospheric NCC reduction for both RCP6.0 (−58%) and RCP8.5 (−44%), albeit the drivers of this reduction are different for the two scenarios: in RCP6.0 the drop in the chemical production is twice that of the loss, thus NCC by the end of the century is smaller than in present-day; while in RCP8.5, although both magnitudes increase, the O₃ loss change is larger than the production change, and consequently NCC is reduced by 2100.

In addition to the projected trends in the chemical production and loss terms, changes in the net sources and sinks of ozone across the tropopause and at the Earth's surface affect the global burden. Future O₃ dry deposition to the Earth's surface declines in RCP6.0 (−21%) and to a lesser extent in RCP8.5 (−6%), mostly

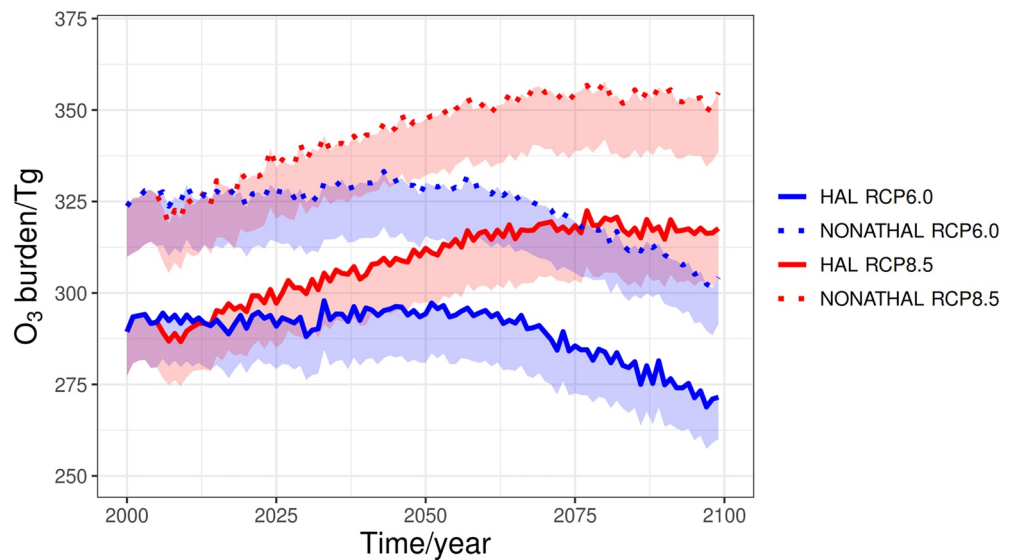


Figure 13. 21st century evolution of the tropospheric ozone burden under Representative Concentration Pathway (RCP)6.0 (blue solid line) and RCP8.5 (red solid line) in comparison with the NONATHAL simulations neglecting tropospheric natural halogen chemistry (dotted lines). Shaded areas indicate the ozone burden range using the two different definitions for the chemical tropopause (between 125 and 150 ppbv). Units are in Tg.

due to a decrease in O_3 levels (for RCP6.0) as well as changes in land cover and other meteorological parameters (i.e., wind speed, temperature, and relative humidity) affecting ozone deposition (Andersson & Engardt, 2010; Kolozsi-Komjáthy et al., 2011). For RCP6.0, slightly larger changes are occurring over water (-23%), while for RCP8.5 the net dry deposition decrease is mostly driven by the dry deposition over land (-9%). Note that dry deposition of NO_y (an important component of the O_3 dry deposition) also decrease in both scenarios due to a significant reduction in NO_x emissions to meet the future air quality standards (Table 2). Our results also indicate a significant increase in STT under both scenarios (41% for RCP6.0 and 56% for RCP8.5) mediated by a strengthened Brewer Dobson circulation under climate change and the future recovery of stratospheric ozone (Collins et al., 2003; Sudo et al., 2003; WMO, 2018). A stratospheric O_3 tracer (O_3S), defined as the amount of O_3 photochemically produced in the stratosphere which is transported and destroyed in the troposphere (Emmons et al., 2003; Roelofs & Lelieveld, 1997; Tao et al., 2018; Wang et al., 1998), is used here to understand the changes in STT during the 21st century (Figure S9 in Supporting Information S1). By computing the changes on the (O_3S/O_3) ratio between 2100 and present time, we find that the future influence of stratospheric O_3 on tropospheric O_3 levels increases globally, particularly in the northern midlatitudes where the upper tropospheric ozone burden is dominated by STT. The overall O_3 burden decreases (-7% to -11%) in RCP6.0 mainly due to reductions in emissions of O_3 precursors. By contrast, under RCP8.5, an increase in stratospheric O_3 influx and an increase in emissions of O_3 precursors (CH_4 and NO_x from lighting) contribute to rise the global tropospheric O_3 burden (7% to 8%).

As described in Section 3.4, ozone changes show a very large regional variability. Indeed, large reductions in surface O_3 toward the end of the century are calculated over United States (~ -15 to -30 ppbv and ~ -10 to -30%), Mediterranean Sea (~ -10 to -25 ppbv and ~ -10 to -20%) and East Asia (~ -5 to -15 ppbv and ~ -10 to -30%) (Figure 11) for both scenarios. However, a significant increase is modeled for Africa (~ 10 – 20 ppb, 20 to 30%) and India (~ 15 – 25 ppb, 15 to 20%) under RCP8.5 (Figure 11). Reductions in chemical loss and dry deposition lead to a slight increase in the lifetime of O_3 under RCP6.0 (21.2 days). By contrast, our calculated lifetime of O_3 is reduced by 1 day (5%) under RCP8.5 (19.8 days) due to the significant increase in the chemical O_3 loss (Table 1).

3.6. Evolution of Tropospheric Ozone Burden and Budget Over This Century

Figure 13 shows the timeline evolution of tropospheric ozone burden during this century for the current simulation (HAL) and a version of our model without tropospheric natural halogen chemistry (NONATHAL,

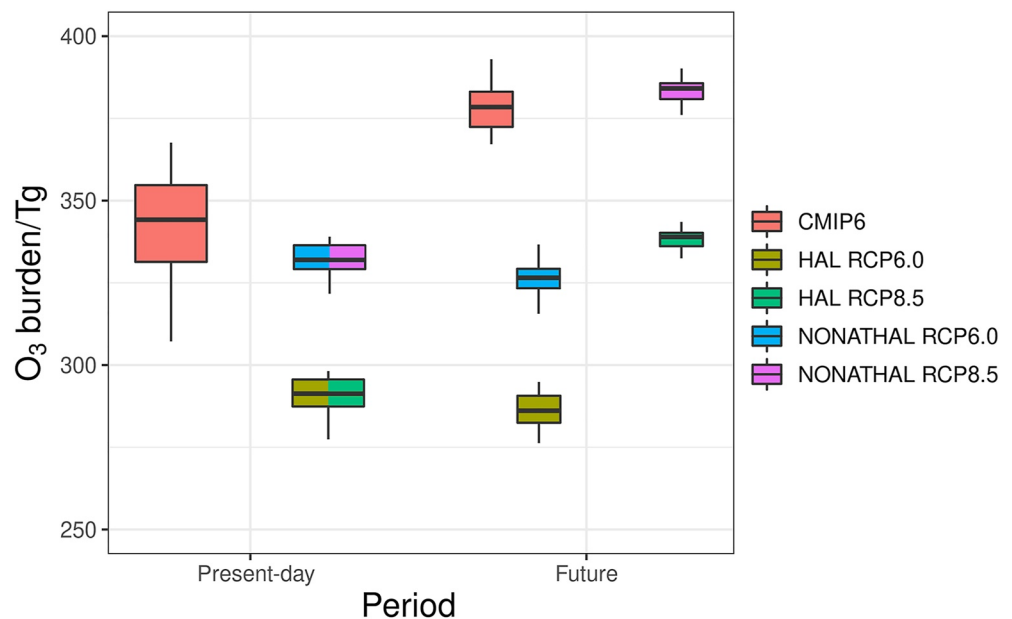


Figure 14. Box-and-whisker plots for the present-day (1990–2009) and end of the century (2080–2099) tropospheric ozone burden under Representative Concentration Pathway (RCP)6.0 and R8.5 for our simulations with and without natural halogens, HAL and NONATHAL, respectively, along with the Phase 6 of the Coupled Model Intercomparison Project (CMIP6) CMIP Historical and ScenarioMIP ssp370 experiments. The tropopause pressure for all models has been defined using the WMO definition. Units are in Tg.

see Section 2.4). The modeled ozone burden for our simulations using the two chemical tropopause definitions (i.e., considering the 150 or 125 ppbv O₃ contour) is shown by the shaded areas in Figure 13. A box-and-whisker plots for the present-day (1990–2009) and end of the century (2080–2099) tropospheric ozone burden under RCP6.0 and R8.5 for our simulations with and without natural halogens, HAL and NONATHAL, respectively, along with the CMIP6 models is presented in Figure 14. For this figure, the WMO tropopause (Reichler et al., 2003) definition is used for all models.

For the RCP6.0 scenario, O₃ burden remains practically constant until 2060 followed by a decrease toward the end of the century. In contrast, the O₃ burden continuously increases until 2060 and then remains relatively flat under RCP8.5. Differences between our model simulations with and without tropospheric natural halogens are significant (~30–35 Tg) and of equivalent magnitude regardless/notwithstanding of the RCP scenario considered, representing between 11% and 15%. Note that research in the last decade has shown the importance of halogen chemistry for tropospheric ozone both in the recent past and present (Badia et al., 2019; MacDonald et al., 2014; Saiz-Lopez et al., 2014; Sherwen et al., 2016; Ziska et al., 2017), as well as during the 21st century (Iglesias-Suarez et al., 2020). Moreover, natural halogen emissions and chemistry have been shown to buffer recent past tropospheric ozone in response to both, climate change and surface ozone precursors (Cuevas et al., 2018). However, current Earth System Models, such as those used in CMIP6, do not include emissions and tropospheric chemistry of halogens. In this sense, Figure 14 shows that the O₃ burdens from our model simulations without natural halogens (NONATHAL) are in line with the CMIP data. Our results show the importance for the modeled present-day O₃ burden—and its change over the century—of including the tropospheric halogen chemistry. Finally, note that our simulations do not include heterogeneous halogen sources and chemistry occurring within the polar regions (Fernandez et al., 2019), thus the presented estimations of the halogen impact on tropospheric ozone burden and lifetime should be considered as a lower limit.

4. Summary and Concluding Remarks

Global emissions of O₃ precursors (CO, NO_x, and NMVOCs) are projected to decline during this century under the RCPs emission scenarios, following long-term strategies to improve air quality and protect human health (Young et al., 2018). This is particularly important over urban sites in United States, Europe, and East Asia where the highest values for health-relevant O₃ concentrations have been measured (Fleming et al., 2018). However, CH₄ emissions under the RCP8.5 scenario are projected to double by the end of this century compared to the present, significantly increasing the future O₃ burden. There is a projected decline in long-lived anthropogenic emissions of halogenated compounds following the Montreal Protocol, whereas natural halogens emitted from the ocean are expected to be very variable in a changing climate (Iglesias-Suarez et al., 2020). Our model results show that a complex interplay of varying natural and anthropogenic emissions, future climate (water vapor and temperature), combined with changes in circulation (deep convection and stronger and Brewer-Dobson circulation), will determine the future chemical processing and distribution of tropospheric O₃ with marked regional asymmetries. We have shown that the largest decrease in the modeled NCC (from −50% to −70%) will occur in the lower troposphere over semi- and polluted coastal regions in the NH (eastern United States, Europe, and eastern Asia), associated with the expected large reductions in O₃ precursor emissions. The abatement in O₃ precursor emissions will, in turn, slow down O₃ production via HO₂ + NO (up to −10% at the surface over the South-East United States) by 2100. In the SH, increases in NCC are projected over Africa, due to increases in future CO and biogenic emissions. Under RCP8.5, O₃ production will increase mostly due to an enhancement in the RO₂ + NO reaction by 2100 compared to present-day. In the upper troposphere (<300 hPa), the modeled tropospheric NCC is projected to increase at the end of the century driven by higher NO_x emissions from lightning and stronger convection, associated to global warming, that transport O₃ precursors to the tropical mid- to upper troposphere. Regarding the net chemical losses, we find that the future evolution of the main chemical O₃ depleting families in the troposphere—HO_x_{loss}, O_x_{loss}, and halogens—will decrease under RCP6.0 following the decline in the tropospheric O₃ burden, mostly during the second half of the century. In contrast, future greater loss contributions by HO_x_{loss}, O_x_{loss}, and Halogens_{loss} cycles are modeled in RCP8.5 as a result of the increase in CH₄ emissions, water vapor, and iodine ocean emissions, respectively. Under RCP6.0, a projected decrease in O₃ production (−12%) results in a decrease of future tropospheric O₃ burden (−7%) with no significant change in O₃ lifetime. In contrast, under RCP8.5 the projected increase in O₃ production (11%) and STT (56%) offsets the increase of O₃ losses (18%), leading to a higher future tropospheric O₃ burden (8%), and a decrease in O₃ lifetime (by 1 day, 5%).

Overall, future surface ozone destruction via halogens relative to the total loss will become more important moving into the future for both scenarios, with up to 5% enhancement respect to the present-day over eastern Asia. Here we show the importance of including tropospheric natural halogen chemistry in Earth System Models used to performed climatic projections of tropospheric ozone by comparing a simulation with and without natural halogen chemistry (30–35 Tg difference in the ozone burden).

Previous studies have found that climate change alone will increase surface O₃ in polluted regions over the 21st century—with the largest increase in urban areas—due to an increase in the frequency of air stagnation episodes (Jacob & Winner, 2009). In the opposite direction, anthropogenically enhanced ocean emissions of reactive halogen species emitted in the form of halocarbons and inorganic iodine will play an important role in future O₃ budgets and tropospheric oxidizing capacity (Iglesias-Suarez et al., 2020). The interplay between the climate penalty—associated with meteorological conditions (e.g., stagnation events)—and enhanced halogen-driven surface O₃ loss will determine the effectiveness of future policies on air quality, and warrants further research. Regardless of the RCP emission considered, we find that tropospheric O₃ NCC will be reduced approximately by half by the end of the century on a global scale, indicating a faster global ozone chemical processing, albeit the changes in future O₃ chemistry and concentrations are projected to be geographically heterogeneous with marked hemispheric, vertical and regional asymmetries. Hence, this study highlights the complexity of understanding, and therefore predicting, the future evolution of tropospheric chemistry and budget, and emphasizes the need for more detailed studies to quantify the effects of climate and emission changes on future air quality in a global and regional scale. Overall, our results also indicate that emission-control policies should take into account future changes in the oxidizing capacity and chemical processing of the atmosphere.

Data Availability Statement

The software code for the CESM model is available from <http://www.cesm.ucar.edu/models/>. Data that support the finding of this study can be downloaded from <http://www.cesm.ucar.edu/models/> and <https://tntcat.iiasa.ac.at/RcpDb/dsd?Action=htmlpage&page=welcome>.

Acknowledgments

This study has received funding from the European Research Council Executive Agency under the European Union's Horizon 2020 Research and Innovation programme (Project "ERC-2016-COG726349 CLIMAHAL"). CAM-Chem is a component of the Community Earth System Model (CESM), which is supported by the NSF and the Office of Science of the US Department of Energy. Computing resources were provided by NCAR's Climate Simulation Laboratory, which is sponsored by the NSF and other agencies. Computing resources, support, and data storage are provided and maintained by the Computational and Information System Laboratory from the National Center of Atmospheric Research (CISSL). Rafael P. Fernandez would like to thank financial support from PICT-2016-0714 (ANPCyT) and i-COOP-B20331 (CSIC + CONICET).

References

- Andersson, C., & Engardt, M. (2010). European ozone in a future climate: Importance of changes in dry deposition and isoprene emissions. *Journal of Geophysical Research*, *115*(D2). <https://doi.org/10.1029/2008JD011690>
- Anenberg, S. C., Horowitz, L. W., Tong, D. Q., & West, J. J. (2010). An estimate of the global burden of anthropogenic ozone and fine particulate matter on premature human mortality using atmospheric modeling. *Environmental Health Perspectives*, *118*(9), 1189–1195. <https://doi.org/10.1289/ehp.0901220>
- Archer, C. L., Brodie, J. F., & Rauscher, S. A. (2019). Global warming will aggravate ozone pollution in the U.S. mid-Atlantic. *Journal of Applied Meteorology and Climatology*, *58*(6), 1267–1278. <https://doi.org/10.1175/JAMC-D-18-0263.1>
- Archibald, A. T., Neu, J. L., Elshorbany, Y. F., Cooper, O. R., Young, P. J., Akiyoshi, H., et al. (2020). Tropospheric ozone assessment report. *Elementa: Science of the Anthropocene*, *8*(1). <https://doi.org/10.1525/elementa.2020.034>
- Archibald, A. T., Turnock, S. T., Griffiths, P. T., Cox, T., Derwent, R. G., Knote, C., & Shin, M. (2020). On the changes in surface ozone over the twenty-first century: Sensitivity to changes in surface temperature and chemical mechanisms. *Philosophical Transactions of the Royal Society A: Mathematical, Physical & Engineering Sciences*, *378*(2183), 20190329. <https://doi.org/10.1098/rsta.2019.0329>
- Atkinson, R. (2003). Kinetics of the gas-phase reactions of OH radicals with alkanes and cycloalkanes. *Atmospheric Chemistry and Physics*, *3*(6), 2233–2307. <https://doi.org/10.5194/acp-3-2233-2003>
- Badia, A., Reeves, C. E., Baker, A. R., Saiz-Lopez, A., Volkamer, R., Koenig, T. K., et al. (2019). Importance of reactive halogens in the tropical marine atmosphere: A regional modelling study using WRF-Chem. *Atmospheric Chemistry and Physics*, *19*(5), 3161–3189. <https://doi.org/10.5194/acp-19-3161-2019>
- Banerjee, A., Maycock, A. C., Archibald, A. T., Abraham, N. L., Telford, P., Braesicke, P., & Pyle, J. A. (2016). Drivers of changes in stratospheric and tropospheric ozone between year 2000 and 2100. *Atmospheric Chemistry and Physics*, *16*(5), 2727–2746. <https://doi.org/10.5194/acp-16-2727-2016>
- Brasseur, G. P., Kiehl, J. T., Müller, J.-F., Schneider, T., Granier, C., Tie, X., & Hauglustaine, D. (1998). Past and future changes in global tropospheric ozone: Impact on radiative forcing. *Geophysical Research Letters*, *25*(20), 3807–3810. <https://doi.org/10.1029/1998GL900013>
- Butchart, N. (2014). The Brewer-Dobson circulation. *Reviews of Geophysics*, *52*(2), 157–184. <https://doi.org/10.1002/2013rg000448>
- Carpenter, L. J., MacDonald, S. M., Shaw, M. D., Kumar, R., Saunders, R. W., Parthipan, R., et al. (2013). Atmospheric iodine levels influenced by sea surface emissions of inorganic iodine. *Nature Geoscience*, *6*(2), 108–111. <https://doi.org/10.1038/ngeo1687>
- Chance, R., Baker, A. R., Carpenter, L., & Jickells, T. D. (2014). The distribution of iodide at the sea surface. *Environmental Sciences: Processes Impacts*, *16*, 1841–1859. <https://doi.org/10.1039/C4EM00139G>
- Collins, W. J., Derwent, R. G., Garnier, B., Johnson, C. E., Sanderson, M. G., & Stevenson, D. S. (2003). Effect of stratosphere-troposphere exchange on the future tropospheric ozone trend. *Journal of Geophysical Research*, *108*(D12). <https://doi.org/10.1029/2002JD002617>
- Crutzen, P. J. (1974). Photochemical reactions initiated by and influencing ozone in unpolluted tropospheric air. *Tellus*, *26*(1–2), 47–57. <https://doi.org/10.1111/j.2153-3490.1974.tb01951.x>
- Cuevas, C. A., Maffezzoli, N., Corella, J. P., Spolaor, A., Vallelonga, P., Kjær, H. A., et al. (2018). Rapid increase in atmospheric iodine levels in the North Atlantic since the mid-20th century. *Nature Communications*, *9*(1), 1452. <https://doi.org/10.1038/s41467-018-03756-1>
- Danabasoglu, G. (2019). *NCAR CESM2-WACCM model output prepared for CMIP6 CMIP*. Earth System Grid Federation. <https://doi.org/10.22033/ESGF/CMIP6.10024>
- Derwent, R., Jenkin, M., & Saunders, S. (1996). Photochemical ozone creation potentials for a large number of reactive hydrocarbons under European conditions. *Atmospheric Environment*, *30*(2), 181–199. [https://doi.org/10.1016/1352-2310\(95\)00303-G](https://doi.org/10.1016/1352-2310(95)00303-G)
- Emmons, L. K., Hess, P., Klonecki, A., Tie, X., Horowitz, L., Lamarque, J.-F., et al. (2003). Budget of tropospheric ozone during TOPSE from two chemical transport models. *Journal of Geophysical Research*, *108*(D8). <https://doi.org/10.1029/2002JD002665>
- Emmons, L. K., Walters, S., Hess, P. G., Lamarque, J.-F., Pfister, G. G., Fillmore, D., et al. (2010). Description and evaluation of the Model for Ozone and Related chemical Tracers, version 4 (MOZART-4). *Geoscientific Model Development*, *3*(1), 43–67. <https://doi.org/10.5194/gmd-3-43-2010>
- Eyring, V., Isaksen, I. S., Bernsten, T., Collins, W. J., Corbett, J. J., Endresen, O., et al. (2010). Transport impacts on atmosphere and climate: Shipping. *Atmospheric Environment*, *44*(37), 4735–4771. (Transport Impacts on Atmosphere and Climate: The ATTICA Assessment Report). <https://doi.org/10.1016/j.atmosenv.2009.04.059>
- Fernandez, R. P., Carmona-Balea, A., Cuevas, C. A., Barrera, J. A., Kinnison, D. E., Lamarque, J.-F., et al. (2019). Modeling the sources and chemistry of polar tropospheric halogens (Cl, Br, and I) using the CAM-Chem global chemistry-climate model. *Journal of Advances in Modeling Earth Systems*, *11*(7), 2259–2289. <https://doi.org/10.1029/2019ms001655>
- Fernandez, R. P., Salawitch, R. J., Kinnison, D. E., Lamarque, J.-F., & Saiz-Lopez, A. (2014). Bromine partitioning in the tropical tropopause layer: Implications for stratospheric injection. *Atmospheric Chemistry and Physics*, *14*(24), 13391–13410. <https://doi.org/10.5194/acp-14-13391-2014>
- Finney, D. L., Doherty, R. M., Wild, O., Young, P. J., & Butler, A. (2016). Response of lightning NO_x emissions and ozone production to climate change: Insights from the Atmospheric Chemistry and Climate Model Intercomparison Project. *Geophysical Research Letters*, *43*(10), 5492–5500. <https://doi.org/10.1002/2016GL068825>
- Fishman, J., Ramanathan, V., Crutzen, P. J., & Liu, S. C. (1979). Tropospheric ozone and climate. *Nature*, *282*, 1476–4687. <https://doi.org/10.1038/282818a0>
- Fleming, Z., Doherty, R., von Schneidemesser, E., Malley, C., Cooper, O., Pinto, J., et al. (2018). Tropospheric ozone assessment report: Present-day ozone distribution and trends relevant to human health. *Elementa: Science of the Anthropocene*, *6*(1), 12. <https://doi.org/10.1525/elementa.273>
- Ganzeveld, L., Bouwman, L., Stehfest, E., van Vuuren, D. P., Eickhout, B., & Lelieveld, J. (2010). Impact of future land use and land cover changes on atmospheric chemistry-climate interactions. *Journal of Geophysical Research*, *115*(D23). <https://doi.org/10.1029/2010JD014041>

- Gaudel, A., Cooper, O. R., Ancellet, G., Barret, B., Boynard, A., Burrows, J. P., et al. (2018). Tropospheric ozone assessment report: Present-day distribution and trends of tropospheric ozone relevant to climate and global atmospheric chemistry model evaluation. *Elementa: Science of the Anthropocene*, 6(1), 39. <https://doi.org/10.1525/elementa.291>
- Griffiths, P. T., Murray, L. T., Zeng, G., Shin, Y. M., Abraham, N. L., Archibald, A. T., et al. (2021). Tropospheric ozone in CMIP6 simulations. *Atmospheric Chemistry and Physics*, 21(5), 4187–4218. <https://doi.org/10.5194/acp-21-4187-2021>
- Hossaini, R., Atlas, E., Dhomse, S. S., Chipperfield, M. P., Bernath, P. F., Fernando, A. M., et al. (2019). Recent trends in stratospheric chlorine from very short-lived substances. *Journal of Geophysical Research: Atmospheres*, 124(4), 2318–2335. <https://doi.org/10.1029/2018JD029400>
- Hossaini, R., Chipperfield, M. P., Saiz-Lopez, A., Fernandez, R., Monks, S., Feng, W., et al. (2016). A global model of tropospheric chlorine chemistry: Organic versus inorganic sources and impact on methane oxidation. *Journal of Geophysical Research: Atmospheres*, 121(23), 14271–14297. <https://doi.org/10.1002/2016JD025756>
- Hsu, J., & Prather, M. J. (2009). Stratospheric variability and tropospheric ozone. *Journal of Geophysical Research*, 114(D6). <https://doi.org/10.1029/2008JD010942>
- Iglesias-Suarez, F., Badia, A., Fernandez, R. P., Cuevas, C. A., Kinnison, D. E., Tilmes, S., et al. (2020). Natural halogens buffer tropospheric ozone in a changing climate. *Nature Climate Change*. <https://doi.org/10.1038/s41558-019-0675-6>
- Iglesias-Suarez, F., Kinnison, D. E., Rap, A., Maycock, A. C., Wild, O., & Young, P. J. (2018). Key drivers of ozone change and its radiative forcing over the 21st century. *Atmospheric Chemistry and Physics*, 18(9), 6121–6139. <https://doi.org/10.5194/acp-18-6121-2018>
- Jacob, D. J., & Winner, D. A. (2009). Effect of climate change on air quality. *Atmospheric Environment*, 43(1), 51–63. (Atmospheric Environment - Fifty Years of Endeavour). <https://doi.org/10.1016/j.atmosenv.2008.09.051>
- Johnson, C. E., Collins, W. J., Stevenson, D. S., & Derwent, R. G. (1999). Relative roles of climate and emissions changes on future tropospheric oxidant concentrations. *Journal of Geophysical Research*, 104(D15), 18631–18645. <https://doi.org/10.1029/1999JD900204>
- Kolozsi-Komjáthy, E., Mészáros, R., & Lagzi, I. (2011). Effects of the climate change on regional ozone dry deposition. *Advances in Science and Research*, 6(1), 103–107. <https://doi.org/10.5194/asr-6-103-2011>
- Krasting, J. P., John, J. G., Blanton, C., McHugh, C., Nikonov, S., Radhakrishnan, A., et al. (2018). NOAA-GFDL GFDL-ESM4 model output prepared for CMIP6 CMIP historical. Earth System Grid Federation. <https://doi.org/10.22033/ESGF/CMIP6.8597>
- Lamarque, J.-F., Emmons, L. K., Hess, P. G., Kinnison, D. E., Tilmes, S., Vitt, F., et al. (2012). CAM-Chem: Description and evaluation of interactive atmospheric chemistry in the Community Earth System Model. *Geoscientific Model Development*, 5(2), 369–411. <https://doi.org/10.5194/gmd-5-369-2012>
- Li, Q., Badia, A., Fernandez, R. P., Mahajan, A. S., López-Noreña, A. L., Zhang, Y., et al. (2021). Chemical interactions between ship-originated air pollutants and ocean-emitted halogens. *Journal of Geophysical Research: Atmospheres*, 126(4), e2020JD034175. <https://doi.org/10.1029/2020jd034175>
- Liu, G., Liu, J., Tarasick, D. W., Fioletov, V. E., Jin, J. J., Moeni, O., et al. (2013). A global tropospheric ozone climatology from trajectory-mapped ozone soundings. *Atmospheric Chemistry and Physics*, 13(21), 10659–10675. <https://doi.org/10.5194/acp-13-10659-2013>
- Liu, J., Tarasick, D. W., Fioletov, V. E., McLinden, C., Zhao, T., Gong, S., et al. (2013). A global ozone climatology from ozone soundings via trajectory mapping: A stratospheric perspective. *Atmospheric Chemistry and Physics*, 13(22), 11441–11464. <https://doi.org/10.5194/acp-13-11441-2013>
- MacDonald, S. M., Gómez Martín, J. C., Chance, R., Warriner, S., Saiz-Lopez, A., Carpenter, L. J., & Plane, J. M. C. (2014). A laboratory characterisation of inorganic iodine emissions from the sea surface: Dependence on oceanic variables and parameterisation for global modelling. *Atmospheric Chemistry and Physics*, 14(11), 5841–5852. <https://doi.org/10.5194/acp-14-5841-2014>
- Mahajan, A. S., Li, Q., Inamdar, S., Ram, K., Badia, A., & Saiz-Lopez, A. (2021). Modelling the impacts of iodine chemistry on the northern Indian Ocean marine boundary layer. *Atmospheric Chemistry and Physics*, 21(11), 8437–8454. <https://doi.org/10.5194/acp-21-8437-2021>
- Meinshausen, M., Smith, S. J., Calvin, K., Daniel, J. S., Kainuma, M. L. T., Lamarque, J.-F., et al. (2011). The RCP greenhouse gas concentrations and their extensions from 1765 to 2300. *Climatic Change*, 109(1), 213. <https://doi.org/10.1007/s10584-011-0156-z>
- Monks, P. S., Archibald, A. T., Colette, A., Cooper, O., Coyle, M., Derwent, R., et al. (2015). Tropospheric ozone and its precursors from the urban to the global scale from air quality to short-lived climate forcer. *Atmospheric Chemistry and Physics*, 15(15), 8889–8973. <https://doi.org/10.5194/acp-15-8889-2015>
- Morgenstern, O., Hegglin, M. I., Rozanov, E., O'Connor, F. M., Abraham, N. L., Akiyoshi, H., et al. (2017). Review of the global models used within phase 1 of the Chemistry–Climate Model Initiative (CCMI). *Geoscientific Model Development*, 10(2), 639–671. <https://doi.org/10.5194/gmd-10-639-2017>
- Murray, C. J. L., Aravkin, A. Y., Zheng, P., Abbafati, C., Abbas, K. M., Abbasi-Kangevari, M., et al. (2020). Global burden of 87 risk factors in 204 countries and territories, 1990–2019: A systematic analysis for the Global Burden of Disease Study 2019. *The Lancet*, 396(10258), 1223–1249. [https://doi.org/10.1016/S0140-6736\(20\)30752-2](https://doi.org/10.1016/S0140-6736(20)30752-2)
- Myhre, G., Shindell, D., Bréon, F.-M., Collins, W., Fuglestedt, J., Huang, J., et al. (2013). Anthropogenic and natural radiative forcing. In *Climate change 2013: The physical science basis. Contribution of working group I to the fifth assessment report of the intergovernmental panel on climate change* (pp. 659–740). Cambridge University Press. <https://doi.org/10.1017/CBO9781107415324.018>
- Neu, J. L., Flury, T., Manney, G. L., Santee, M. L., Livesey, N. J., & Worden, J. (2014). Tropospheric ozone variations governed by changes in stratospheric circulation. *Nature Geoscience*, 7(5), 340–344. <https://doi.org/10.1038/ngeo2138>
- Ordóñez, C., Lamarque, J.-F., Tilmes, S., Kinnison, D. E., Atlas, E. L., Blake, D. R., et al. (2012). Bromine and iodine chemistry in a global chemistry-climate model: Description and evaluation of very short-lived oceanic sources. *Atmospheric Chemistry and Physics*, 12(3), 1423–1447. <https://doi.org/10.5194/acp-12-1423-2012>
- Prados-Roman, C., Cuevas, C. A., Hay, T., Fernandez, R. P., Mahajan, A. S., Royer, S.-J., et al. (2015). Iodine oxide in the global marine boundary layer. *Atmospheric Chemistry and Physics*, 15(2), 583–593. <https://doi.org/10.5194/acp-15-583-2015>
- Prather, M. J., Zhu, X., Tang, Q., Hsu, J., & Neu, J. L. (2011). An atmospheric chemist in search of the tropopause. *Journal of Geophysical Research*, 116(D4). <https://doi.org/10.1029/2010JD014939>
- Read, K. A., Mahajan, A. S., Carpenter, L. J., Evans, M. J., Faria, B. V. E., Heard, D. E., et al. (2008). Extensive halogen-mediated ozone destruction over the tropical Atlantic Ocean. *Nature*, 453(7199), 1232–1235. <https://doi.org/10.1038/nature07035>
- Reichler, T., Dameris, M., & Sausen, R. (2003). Determining the tropopause height from gridded data. *Geophysical Research Letters*, 30(20). <https://doi.org/10.1029/2003GL018240>
- Roelofs, G.-J., & Lelieveld, J. (1997). Model study of the influence of cross-tropopause O₃ transports on tropospheric O₃ levels. *Tellus B: Chemical and Physical Meteorology*, 49(1), 38–55. <https://doi.org/10.1034/j.1600-0889.49.issue1.3.x>
- Saiz-Lopez, A., Baidar, S., Cuevas, C. A., Koenig, T. K., Fernandez, R. P., Dix, B., et al. (2015). Injection of iodine to the stratosphere. *Geophysical Research Letters*, 42(16), 6852–6859. <https://doi.org/10.1002/2015GL064796>

- Saiz-Lopez, A., Fernandez, R. P., Ordóñez, C., Kinnison, D. E., Gómez Martín, J. C., Lamarque, J.-F., & Tilmes, S. (2014). Iodine chemistry in the troposphere and its effect on ozone. *Atmospheric Chemistry and Physics*, *14*(23), 13119–13143. <https://doi.org/10.5194/acp-14-13119-2014>
- Saiz-Lopez, A., & von Glasow, R. (2012). Reactive halogen chemistry in the troposphere. *Chemical Society Reviews*, *41*, 6448–6472. <https://doi.org/10.1039/C2CS35208G>
- Sander, S. P., Friedl, R. R., Abbatt, J. P. D., Barker, J. R., Burkholder, J. B., Golden, D. M., et al. (2011). *Chemical kinetics and photochemical data for use in atmospheric studies, evaluation number 17* (Technical report).
- Schultz, M. G., Schröder, S., Lyapina, O., Cooper, O., Galbally, I., Petropavlovskikh, I., et al. (2017). Tropospheric ozone assessment report: Database and metrics data of global surface ozone observations. *Elementa: Science of the Anthropocene*, *5*(0), 58. <https://doi.org/10.1525/elementa.244>
- Sellar, A. A., Jones, C. G., Mulcahy, J. P., Tang, Y., Yool, A., Wiltshire, A., et al. (2019). UKESM1: Description and evaluation of the U.K. Earth System Model. *Journal of Advances in Modeling Earth Systems*, *11*(12), 4513–4558. <https://doi.org/10.1029/2019MS001739>
- Sherwen, T., Schmidt, J. A., Evans, M. J., Carpenter, L. J., Großmann, K., Eastham, S. D., et al. (2016). Global impacts of tropospheric halogens (Cl, Br, I) on oxidants and composition in GEOS-Chem. *Atmospheric Chemistry and Physics*, *16*(18), 12239–12271. <https://doi.org/10.5194/acp-16-12239-2016>
- Sillman, S. (2003). 9.11—Tropospheric ozone and photochemical smog. In H. D. Holland, & K. K. Turekian (Eds.), *Treatise on geochemistry* (pp. 407–431). Pergamon. <https://doi.org/10.1016/B0-08-043751-6/09053-8>
- Stevenson, D. S., Dentener, F. J., Schultz, M. G., Ellingsen, K., van Noije, T. P. C., Wild, O., et al. (2006). Multimodel ensemble simulations of present-day and near-future tropospheric ozone. *Journal of Geophysical Research*, *111*(D8). <https://doi.org/10.1029/2005JD006338>
- Stevenson, D. S., Johnson, C. E., Collins, W. J., Derwent, R. G., & Edwards, J. M. (2000). Future estimates of tropospheric ozone radiative forcing and methane turnover—The impact of climate change. *Geophysical Research Letters*, *27*(14), 2073–2076. <https://doi.org/10.1029/1999GL010887>
- Stohl, A., Bonasoni, P., Cristofanelli, P., Collins, W., Feichter, J., Frank, A., et al. (2003). Stratosphere-troposphere exchange: A review, and what we have learned from STACCATO. *Journal of Geophysical Research*, *108*(D12). <https://doi.org/10.1029/2002JD002490>
- Sudo, K., Takahashi, M., & Akimoto, H. (2003). Future changes in stratosphere-troposphere exchange and their impacts on future tropospheric ozone simulations. *Geophysical Research Letters*, *30*(24). <https://doi.org/10.1029/2003GL018526>
- Tao, M., Pan, L. L., Konopka, P., Honomichl, S. B., Kinnison, D. E., & Apel, E. C. (2018). A Lagrangian model diagnosis of stratospheric contributions to tropical midtropospheric air. *Journal of Geophysical Research: Atmospheres*, *123*(17), 9764–9785. <https://doi.org/10.1029/2018JD028696>
- Tarasick, D. W., Galbally, I., Cooper, O., Schultz, M., Ancellet, G., Leblanc, T., et al. (2019). Tropospheric ozone assessment report: Tropospheric ozone from 1877 to 2016, observed levels, trends and uncertainties. *Elementa: Science of the Anthropocene*, *7*(1), 39. <https://doi.org/10.1525/elementa.376>
- Tarasick, D. W., Jin, J. J., Fioletov, V. E., Liu, G., Thompson, A. M., Oltmans, S. J., et al. (2010). High-resolution tropospheric ozone fields for INTEX and ARCTAS from IONS ozonesondes. *Journal of Geophysical Research*, *115*(D20). <https://doi.org/10.1029/2009JD012918>
- Tilmes, S., Lamarque, J.-F., Emmons, L. K., Kinnison, D. E., Ma, P.-L., Liu, X., et al. (2015). Description and evaluation of tropospheric chemistry and aerosols in the Community Earth System Model (CESM1.2). *Geoscientific Model Development*, *8*(5), 1395–1426. <https://doi.org/10.5194/gmd-8-1395-2015>
- Tilmes, S., Lamarque, J.-F., Emmons, L. K., Kinnison, D. E., Marsh, D., Garcia, R. R., et al. (2016). Representation of the Community Earth System Model (CESM1) CAM4-Chem within the Chemistry-Climate Model Initiative (CCMI). *Geoscientific Model Development*, *9*(5), 1853–1890. <https://doi.org/10.5194/gmd-9-1853-2016>
- van Vuuren, D. P., Edmonds, J., Kainuma, M., Riahi, K., Thomson, A., Hibbard, K., et al. (2011). The representative concentration pathways: An overview. *Climatic Change*, *109*(1), 5. <https://doi.org/10.1007/s10584-011-0148-z>
- Wang, Y., Jacob, D. J., & Logan, J. A. (1998). Global simulation of tropospheric O₃-NO_x-hydrocarbon chemistry: 1. Model formulation. *Journal of Geophysical Research*, *103*(D9), 10713–10725. <https://doi.org/10.1029/98JD00158>
- Wild, O. (2007). Modelling the global tropospheric ozone budget: Exploring the variability in current models. *Atmospheric Chemistry and Physics*, *7*(10), 2643–2660. <https://doi.org/10.5194/acp-7-2643-2007>
- WMO. (2011). *Scientific assessment of ozone depletion: 2010* (Technical report, Global Ozone Research and Monitoring Project-Report No. 52). World Meteorological Organization.
- WMO. (2018). *Scientific assessment of ozone depletion: 2018* (Technical report, Global Ozone Research and Monitoring Project-Report No. 58, p. 588). World Meteorological Organization.
- Young, P. J., Archibald, A. T., Bowman, K. W., Lamarque, J.-F., Naik, V., Stevenson, D. S., et al. (2013). Pre-industrial to end 21st century projections of tropospheric ozone from the Atmospheric Chemistry and Climate Model Intercomparison Project (ACCMIP). *Atmospheric Chemistry and Physics*, *13*(4), 2063–2090. <https://doi.org/10.5194/acp-13-2063-2013>
- Young, P. J., Naik, V., Fiore, A. M., Gaudel, A., Guo, J., Lin, M. Y., et al. (2018). Tropospheric ozone assessment report: Assessment of global-scale model performance for global and regional ozone distributions, variability, and trends. *Elementa: Science of the Anthropocene*, *6*(1), 10. <https://doi.org/10.1525/elementa.265>
- Yukimoto, S., Koshiro, T., Kawai, H., Oshima, N., Yoshida, K., Urakawa, S., et al. (2019). *MRI MRI-ESM2.0 model output prepared for CMIP6 CMIP*. Earth System Grid Federation. <https://doi.org/10.22033/ESGF/CMIP6.621>
- Zeng, G., Pyle, J. A., & Young, P. J. (2008). Impact of climate change on tropospheric ozone and its global budgets. *Atmospheric Chemistry and Physics*, *8*(2), 369–387. <https://doi.org/10.5194/acp-8-369-2008>
- Ziska, F., Quack, B., Tegtmeier, S., Stemmler, I., & Krüger, K. (2017). Future emissions of marine halogenated very-short lived substances under climate change. *Journal of Atmospheric Chemistry*, *74*(2), 245–260. <https://doi.org/10.1007/s10874-016-9355-3>